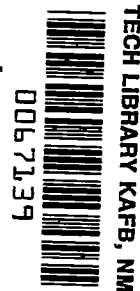# NATIONAL ADVISORY COMMITTEE
FOR AERONAUTICS

TECHNICAL NOTE 3943

A POWER-SERIES SOLUTION FOR THE UNSTEADY LAMINAR

BOUNDARY-LAYER FLOW IN AN EXPANSION WAVE

OF FINITE WIDTH MOVING THROUGH

A GAS INITIALLY AT REST

By Nathaniel B. Cohen

Langley Aeronautical Laboratory
Langley Field, Va.

NACA

1Z

NATIONAL ADVISORY COMMITTEE FOR AERONAUTI.

TECHNICAL NOTE 3943

A POWER-SERIES SOLUTION FOR THE UNSTEADY LAMINAR

BOUNDARY-LAYER FLOW IN AN EXPANSION WAVE

OF FINITE WIDTH MOVING THROUGH

A GAS INITIALLY AT REST

By Nathaniel B. Cohen

SUMMARY

The equations of motion and energy for the laminary boundary-layer
flow in an expansion wave of finite width moving into undisturbed fluid,
such as in a shock tube, were considered. Solutions in the form of
infinite power series for velocity and local enthalpy functions were
indicated, and the first three terms of each series were numerically
evaluated. Validity of the numerical results was restricted to the
region near the leading edge of the expansion wave. Skin friction and
heat transfer were compared with values given by a solution which con-
sidered the expansion wave as equivalent to a line discontinuity across
which existence of isentropic expansion relations was assumed. These
solutions were shown to be very different, qualitatively as well as
quantitatively. Singularities in the flow field were discussed in
regard to both the finite-width expansion-wave and the line-expansion-
wave solutions.

INTRODUCTION

Extensive use of shock tubes for aerodynamic research has placed
emphasis upon the effects of using a real, rather than a perfect, gas.
The flow phenomena for an ideal fluid are easily derived and are given,
for example, in references 1 to 3. Deviations from the ideal flow may
occur because the working fluid is imperfect and because fluid viscosity
and thermal conductivity introduce effects of the shock-tube walls upon
the flow. For moderate shock-pressure ratios, imperfect gas effects may
be neglected, but the wall effects may remain important; the present
analysis considers only the fluid viscosity and conductivity.

Deviations from ideal shock-tube flow are most easily seen experi-
mentally through measurements of the shock-wave velocity. Experimental

attenuations in shock strength were investigated in references 1, 2, 4, 5, and 6. Reference 6 also presented measurements of static-pressure variations with time at a fixed position after passage of the shock wave. Experimental timewise density variations in the flow through the use of a chrono-interferometer were shown in reference 7.

Various theoretical studies have been carried out as well. References 1 and 4 considered a reduction in mass flow at the entropy discontinuity computed from the boundary-layer displacement thickness and the free stream corresponding to the unattenuated shock. Attenuation in the shock strength was then found by setting the mass flow through the shock wave equal to the reduced mass flow at the entropy discontinuity and computing the new shock strength. The unsteady laminary boundary layer in the hot gas behind the shock was derived in reference 2, and the resulting skin-friction and heat-transfer effects averaged across the assumed one-dimensional flow. The attenuation resulting from the waves generated at the entropy discontinuity by these boundary-layer effects were then computed.

In reference 6, waves generated throughout the entire shock tube by skin-friction and heat-transfer effects were considered to affect the real gas flow, average skin-friction and heat-transfer coefficients being based upon incompressible, turbulent, steady-flow flat-plate boundary-layer values. The expansion wave was treated as a line discontinuity across which isentropic relations were assumed to be valid (zero-thickness expansion wave). Experimental data have shown excellent agreement with this theory.

The assumption of the equivalence of steady- and unsteady-flow laminar boundary layers was shown to be rather inaccurate by the unsteady laminar boundary-layer theories of references 2, 8, and 9, which treated the exact boundary-layer equations for the flow behind a shock wave moving into an undisturbed fluid. Reference 9 extended the theory to laminar flow behind a zero-thickness expansion wave and presented solutions to the integrated equations of motion and energy for laminar and turbulent boundary layers behind both shock and zero-thickness expansion waves. The boundary-layer theories of references 8 and 9 have been incorporated into a theory predicting shock-wave attenuation in a shock tube (ref. 10).

The turbulent boundary layer in an expansion wave of finite width (expansion fan) was considered on an equivalent steady-flow basis in reference 11, but only recently has any attempt been made to investigate the unsteady boundary layer for this case. Reference 12 presents a solution to the complete shock-tube boundary-layer problem, including the fan, for laminar compressible flow. The integrated equations of motion and energy are considered and graphical and numerical isoclinal procedures are utilized. A feature of this theory is the use of the method of characteristics to obtain the solution, a necessity because singularities originating at the time of diaphragm burst propagate through the shock-tube flow field.

The present paper presents an approximate solution to the differential boundary-layer equations of motion and energy for the unsteady laminar flow of a compressible fluid under the influence of the ideal-fluid expansion-fan pressure gradient. Results are compared with the results of the expansion-discontinuity analysis of reference 9. Much of the material presented herein was submitted to the University of Virginia in partial fulfillment of the requirements for a Master of Aeronautical Engineering degree.

SYMBOLS

a local velocity of sound

C_w function defined by $\left(\dfrac{T_w}{T_1}\right)^{0.5}\left(\dfrac{T_1 + S}{T_w + S}\right)$

C_ϵ function defined by $\left(\dfrac{T_\epsilon}{T_1}\right)^{0.5}\left(\dfrac{T_1 + S}{T_\epsilon + S}\right)$

c_p coefficient of specific heat at constant pressure

c_v coefficient of specific heat at constant volume

F_n particular function of nth-order differential equation of motion

f dimensionless stream function

f_n nth-order term in power-series representation of f

G_n particular function of nth-order differential energy equation

g dimensionless enthalpy function

g_n nth-order term in power-series representation of g

h local enthalpy

h^* enthalpy difference, $h - h_w$

h_0 stagnation enthalpy

k thermal conductivity

N_{Pr} Prandtl number

p   static pressure

R   gas constant

q   rate of heat transfer

$$\hat{q}_w = \frac{q_w}{\rho_\epsilon a_\epsilon^2 \sqrt{\dfrac{\nu_\epsilon}{\bar{t}}}}$$

$$\bar{q}_w = \frac{q_w}{\rho_w \dfrac{h_1^*}{N_{Pr}} \sqrt{\dfrac{\nu_\epsilon}{\bar{t}\xi}}}$$

S   constant in Sutherland viscosity-temperature relation

T   temperature

$t, \bar{t}$ time

u   velocity of fluid in x- or $\bar{x}$-direction

u_W wave velocity

u_s shock velocity

v   velocity of fluid in Y- or y-direction

$x, \bar{x}$ coordinate along wall

Y   "incompressible" coordinate normal to wall, $\displaystyle\int_0^y \frac{\rho}{\rho_\epsilon}\,dy$

y   coordinate normal to wall

γ ratio of specific heats, c_p/c_v

η dimensionless coordinate, $\dfrac{Y}{\sqrt{\nu_\epsilon \xi \bar{t}}}$

μ absolute viscosity

ν kinematic viscosity

ξ dimensionless coordinate, $1 - \dfrac{\bar{x}}{u_w \bar{t}}$

ξ_{te} coordinate ξ evaluated at trailing edge of expansion fan

ρ density

τ shear stress

$$\hat{\tau}_w = \frac{\tau_w}{\rho_\epsilon a_\epsilon \sqrt{\dfrac{\nu_\epsilon}{\bar{t}}}}$$

$$\bar{\tau}_w = \frac{\tau_w}{\rho_w u_1 \sqrt{\dfrac{\nu_\epsilon}{\bar{t}\xi}}}$$

ψ stream function

θ, φ dummy variable of integration

Subscripts:

n   index of order of term in power series

w   quantity evaluated at wall $(y = 0)$

α quantity evaluated in shock-tube region α, cold gas (see
             fig. 1(a))

β quantity evaluated in shock-tube region β, hot gas (see
             fig. 1(a))

ϵ quantity evaluated in shock-tube undisturbed reference
             state ϵ (see fig. 1(a))

1   quantity evaluated in free stream $(y \rightarrow \infty)$

∞ quantity evaluated in shock tube undisturbed low-pressure
             region ∞ (see fig. 1(a))

Quantities written with a bar underneath are dimensionless with
respect to the appropriate quantity in the undisturbed region ϵ; for
example, $\underline{u} = \dfrac{u}{a_\epsilon}$, $\underline{p}_1 = \dfrac{p_1}{p_\epsilon}$, and so forth.

Primes denote total differentiation of the functions $f_n(\eta)$ and
$g_n(\eta)$ with respect to the argument η.

THEORY

The Prandtl boundary-layer equations are reduced to a system of two simultaneous, nonlinear, partial differential equations involving unsteady stream and enthalpy functions through a transformation of coordinates. The special case of flow in an expansion fan advancing into a fluid at rest is considered. Solutions in the form of infinite power series are assumed, and each partial differential equation is reduced to an infinite number of ordinary differential equations.

Assumptions

The assumptions necessary to the analysis which follows are:

1. The Prandtl boundary-layer equations are assumed to be valid for the expansion fan, which is considered as centered, that is, originating at a single point on the x,t plane. A shock-tube wave diagram of the ideal-fluid flow for an expansion fan of moderate strength is shown in figure 1(a). Figure 1(b) illustrates qualitatively the corresponding boundary layer. The point of origin of the fan at $x = t = 0$ (representing, for example, the diaphragm burst in a shock tube) is a singular point and must be excluded from the analysis. The trailing edge of the expansion fan, separating the fan and the region of constant fluid properties (region α in fig. 1(a)), represents a discontinuity in the derivatives of the stream quantities and thus also violates the boundary-layer assumptions. Distortion of the trailing edge caused by varying the velocity and temperature within the boundary layer is neglected.

In the region near the leading edge of the fan the velocity is low and increases linearly in the ratio x/t from a value of zero at the leading edge. This situation appears analogous to the region near the forward stagnation point of a blunt body in steady flow and the Prandtl boundary-layer assumptions, through this analogy, are assumed to hold in this region. Therefore, the boundary-layer equations are assumed to be valid in the expansion fan except at the origin and along the free-stream trailing edge.

One additional restriction on the use of the boundary-layer equations must be noted for the special case of shock-tube flow. For a strong expansion process, part of the expansion fan occurs in the region where $x > 0$. The "no-slip" boundary condition at the wall requires that the temperature discontinuity separating the hot gas of region β from the cold gas of region α remain in the boundary layer extending back to the position of the diaphragm. This case is illustrated in the ideal-fluid wave diagram (fig. 2(a)) and in the corresponding boundary-layer formation (fig. 2(b)). At some time after the diaphragm burst, laminar

diffusion will have acted to smooth the discontinuity to some extent, but large streamwise temperature gradients will still exist in the region near the position of the discontinuity in the free stream. This condition precludes application of the Prandtl boundary-layer equations. Elsewhere in the region between $x = 0$ and the discontinuity, turning of the discontinuity surface toward the wall will probably have reduced the streamwise temperature gradient sufficiently for the boundary-layer equations to apply. Since the trailing edge of the fan always lies upstream of the discontinuity, it is assumed herein that streamwise temperature gradients large enough to invalidate the boundary-layer equations never exist inside the expansion fan.

2. The coefficients of specific heat, c_p and c_v , and the Prandtl number are assumed to be constant.

3. A linear viscosity-temperature relation is assumed. The constant of proportionality is defined so that the correct wall viscosity is used; the error introduced elsewhere in the boundary layer is neglected.

4. The wall temperature is assumed to be constant. Because walls are generally constructed of materials for which values of thermal conductivity and heat capacity per unit volume are high when compared with the values for the gas, this assumption, which has been shown to be valid for flow behind a shock in reference 9, should be reasonably good for the expansion-fan analysis.

The Basic Equations of the Fluid Motion

The differential equations governing the unsteady, two-dimensional flow of a compressible, viscous fluid under the Prandtl boundary-layer assumptions are the equation of continuity

$$\frac{\partial \rho}{\partial t} + \frac{\partial (\rho u)}{\partial x} + \frac{\partial (\rho v)}{\partial y} = 0 \qquad (1)$$

the equations of motion

$$\frac{\partial u}{\partial t} + u\frac{\partial u}{\partial x} + v\frac{\partial u}{\partial y} = -\frac{1}{\rho}\frac{\partial p}{\partial x} + \frac{1}{\rho}\frac{\partial}{\partial y}\left(\mu\frac{\partial u}{\partial y}\right) \qquad (2a)$$

$$0 = -\frac{1}{\rho}\frac{\partial p}{\partial y} \qquad (2b)$$

the energy equation for constant N_{Pr} and c_p

$$\frac{\partial h}{\partial t} + u\frac{\partial h}{\partial x} + v\frac{\partial h}{\partial y} = \frac{1}{\rho}\left(\frac{\partial p}{\partial t} + u\frac{\partial p}{\partial x} + v\frac{\partial p}{\partial y}\right) + \frac{1}{\rho N_{Pr}}\frac{\partial}{\partial y}\left(\mu\frac{\partial h}{\partial y}\right) + \nu\left(\frac{\partial u}{\partial y}\right)^2 \qquad (3)$$

and the equation of state

$$p = \rho R T = \frac{\gamma - 1}{\gamma}\rho h \qquad (4)$$

The coordinate system is fixed to the wall, the origin of the x- and t-axes being at the origin of the expansion wave. The use of only two space dimensions, x and y, implies that interactions between adjacent wall boundary layers are neglected.

Equation (2b) immediately yields the result that the pressure is constant across the boundary layer or that

$$p(x,y,t) = p_1(x,t) \qquad (5)$$

Equations (1), (2a), (3), and (4) then are to be solved for the four dependent variables u, v, ρ, h. The appropriate boundary conditions are

$$\left.\begin{array}{l} u(x,0,t) = 0 \\[4pt] u(x,\infty,t) = u_1(x,t) \\[4pt] v(x,0,t) = 0 \\[4pt] h(x,0,t) = h_w(x,t) \\[4pt] h(x,\infty,t) = h_1(x,t) \end{array}\right\} \qquad (6)$$

In order that the equations may be more generally applicable, the enthalpy at the wall is retained as a variable.

The linear viscosity-temperature relation discussed by Chapman and Rubesin (ref. 13) is employed; namely,

$$\frac{\mu}{\mu_1} = C_W(x,t)\frac{T}{T_1} \tag{7}$$

where the proportionality function $C_W(x,t)$ is obtained by requiring that equation (7) satisfy the Sutherland relation at the wall; thus,

$$C_W(x,t) = \left(\frac{T_w}{T_1}\right)^{0.5}\left(\frac{T_1 + S}{T_w + S}\right) \tag{8}$$

A conventional transformation of coordinates and an unsteady stream function are next introduced, the latter function identically satisfying the equation of continuity. The definitions are

$$\left.\begin{array}{l} \bar{x} = x \\[2mm] Y = \displaystyle\int_0^y \frac{\rho(x,y,t)}{\rho_\epsilon}\,dy \\[2mm] \bar{t} = t \\[2mm] u = \dfrac{\rho_\epsilon}{\rho}\dfrac{\partial\psi}{\partial y} = \dfrac{\partial\psi}{\partial Y} \\[2mm] v = -\dfrac{\rho_\epsilon}{\rho}\left(\dfrac{\partial\psi}{\partial x} + \dfrac{\partial}{\partial t}\displaystyle\int_0^y \dfrac{\rho}{\rho_\epsilon}\,dy\right) = -\dfrac{\rho_\epsilon}{\rho}\left(\dfrac{\partial\psi}{\partial\bar{x}} + \dfrac{\partial\psi}{\partial Y}\dfrac{\partial Y}{\partial x} + \dfrac{\partial Y}{\partial t}\right) \end{array}\right\} \tag{9}$$

Equations (5), (7), and the transformation and stream function of equations (9) are then simultaneously substituted into equations (2a) and (3); the resulting equations are, respectively,

$$\frac{\partial^2\psi}{\partial Y\partial\bar{t}} + \frac{\partial\psi}{\partial Y}\frac{\partial^2\psi}{\partial\bar{x}\partial Y} - \frac{\partial\psi}{\partial\bar{x}}\frac{\partial^2\psi}{\partial Y^2} = -\frac{\gamma - 1}{\gamma}\frac{h}{p_1}\frac{\partial p_1}{\partial x} + \frac{\rho_1\mu_1 C_w}{\rho_\epsilon^2}\frac{\partial^3\psi}{\partial Y^3} \tag{10}$$

$$\frac{\partial h}{\partial \bar{t}} + \frac{\partial \psi}{\partial Y} \frac{\partial h}{\partial \bar{x}} - \frac{\partial \psi}{\partial \bar{x}} \frac{\partial h}{\partial Y} = \frac{\gamma - 1}{\gamma} \frac{h}{p_1} \left(\frac{\partial p_1}{\partial \bar{t}} + \frac{\partial \psi}{\partial Y} \frac{\partial p_1}{\partial \bar{x}} \right) + \frac{\rho_1 \mu_1}{\rho_\epsilon^2} \frac{C_w}{N_{Pr}} \frac{\partial^2 h}{\partial Y^2} + \frac{\rho_1 \mu_1 C_w}{\rho_\epsilon^2} \left(\frac{\partial^2 \psi}{\partial Y^2} \right)^2$$

$$(11)$$

The appropriate boundary conditions on the stream function and enthalpy, written in $\bar{x}, Y, \bar{t}$ coordinates, are

$$\left. \left(\frac{\partial \psi}{\partial Y} \right) \right|_{Y=0} = 0$$

$$\left. \left(\frac{\partial \psi}{\partial Y} \right) \right|_{Y \to \infty} = u_1(\bar{x}, \bar{t})$$

$$\psi(\bar{x}, 0, \bar{t}) = 0$$

$$h(\bar{x}, 0, \bar{t}) = h_w(\bar{x}, \bar{t})$$

$$h(\bar{x}, \infty, \bar{t}) = h_1(\bar{x}, \bar{t})$$

$$(12)$$

Equations (10) and (11) and the appropriate boundary conditions of equations (12) thus describe the boundary-layer flow in a very general manner and require only the assumptions of constant c_p and N_{Pr} and a linear viscosity-temperature relation. Solution of a particular problem requires that the boundary conditions be given explicitly and that the differential equations be further reduced. The exact form of the boundary conditions will be shown to influence strongly the methods of simplification of the differential equations.

<center>Timewise Conical Similarity</center>

<u>Similarity transformations</u>.- Listed in appendix A are the potential-flow relations for flow in a centered expansion fan. The equations for u_1 and h_1 are the free-stream boundary conditions for the boundary-layer differential equations and are functions only of the ratio x/t; thus, in a distance-time sense, the expansion-fan potential-flow variables are conical. If, in addition, the wall temperature is assumed to be constant, it is seen from equations (12) that all the wall boundary conditions

satisfy the conical requirement (that is, constancy), and it then appears reasonable to search for solutions containing this conical similarity.

Similar stream and enthalpy functions, f and g, respectively, are defined as

$$\psi(\bar{x},Y,\bar{t}) = u_1(\xi)\sqrt{\nu_\epsilon \xi \bar{t}}\ f(\xi,\eta) \tag{13}$$

$$h(\bar{x},Y,\bar{t}) = h_w + h_1^*(\xi)g(\xi,\eta) \tag{14}$$

where

$$\left.\begin{aligned}\xi &= 1 - \frac{\bar{x}}{u_w \bar{t}} \\[2em] \eta &= \frac{Y}{\sqrt{\nu_\epsilon\left(\bar{t} - \frac{\bar{x}}{u_w}\right)}} = \frac{Y}{\sqrt{\nu_\epsilon \xi \bar{t}}}\end{aligned}\right\} \tag{15}$$

The enthalpy at the wall h_w is herein assumed to be constant. The velocity u_w represents a wave velocity and is used so that, by employing the proper boundary conditions, equations (15) may represent the flow behind a shock as well as in an expansion fan. For the flow behind the shock, the wave velocity is then u_s; for the flow in the expansion fan, the wave velocity is considered to be the velocity of the leading edge of the expansion fan and is equal to $-a_\epsilon$. The parameter ξ is the conical similarity parameter and is defined so that it is zero on the wave. The diffusion parameter η is closely related to that employed in references 2 and 8. This relation may be seen by rewriting the parameter as

$$\eta = \frac{Y}{\sqrt{\frac{\nu_\epsilon}{u_w}(u_w\bar{t} - \bar{x})}} \tag{15a}$$

The length $u_w\bar{t} - \bar{x}$ is equal to the distance from the wave, and the close resemblance of this parameter to that of the references is now evident.

Transformation of coordinates from $\bar{x}, Y, \bar{t}$ to $\xi, \eta, \bar{t}$ through the use of relations (15) and simultaneous introduction of the stream and enthalpy functions (eqs. (13) and (14)) reduce the equations of motion and energy (eqs. (10) and (11), respectively) to the following:

$$\rho_1 \mu_1 C_w \frac{u_1}{\xi} \frac{\partial^3 f}{\partial \eta^3} + \frac{\partial^2 f}{\partial \eta^2}\left[\frac{u_1}{2\xi}\eta - \frac{u_1}{u_w}\left(\frac{du_1}{d\xi}f + \frac{u_1}{2\xi}f + u_1 \frac{\partial f}{\partial \xi}\right)\right] +$$

$$\left[(\xi - 1) + \frac{u_1}{u_w}\frac{\partial f}{\partial \eta}\right]\left(\frac{du_1}{d\xi}\frac{\partial f}{\partial \eta} + u_1 \frac{\partial^2 f}{\partial \eta \partial \xi}\right) + \frac{1}{\gamma}\frac{h_w + h_1^* g}{u_w}\frac{1}{p_1}\frac{dp_1}{d\xi} = 0 \qquad (16)$$

$$\rho_1 \mu_1 C_w\left[\frac{1}{N_{Pr}}\frac{h_1^*}{\xi}\frac{\partial^2 g}{\partial \eta^2} + (\gamma - 1)\frac{u_1^2}{\xi}\left(\frac{\partial^2 f}{\partial \eta^2}\right)^2\right] + h_1^* \frac{\partial g}{\partial \eta}\left[\frac{\eta}{2\xi} - \frac{u_1}{u_w}\left(\frac{1}{u_1}\frac{du_1}{d\xi}f + \right.\right.$$

$$\left.\left. \frac{1}{2\xi}f + \frac{\partial f}{\partial \xi}\right)\right] + \left[(\xi - 1) + \frac{u_1}{u_w}\frac{\partial f}{\partial \eta}\right]\left[\frac{dh_1}{d\xi}g + h_1^* \frac{\partial g}{\partial \xi} - \right.$$

$$\left. \frac{\gamma - 1}{\gamma}\left(h_w + h_1^* g\right)\frac{1}{p_1}\frac{dp_1}{d\xi}\right] = 0 \qquad (17)$$

Boundary conditions are transformed from equations (12) and are

$$\left.\begin{array}{r}
\left(\dfrac{\partial f}{\partial \eta}\right)_{\eta=0} = 0 \\[2ex]
\left(\dfrac{\partial f}{\partial \eta}\right)_{\eta \to \infty} = 1 \\[2ex]
f(\xi, 0) = 0 \\[1ex]
g(\xi, 0) = 0 \\[1ex]
g(\xi, \infty) = 1
\end{array}\right\} \qquad (18)$$

The absence of the independent variable $\bar{t}$ from the differential equations (16) and (17) and from the boundary conditions of equations (18), except implicitly, indicates the existence of solutions exhibiting similarity in ξ and η as was assumed in equations (13) and (14). The number of independent variables has therefore been reduced to two.

Application to the centered expansion fan.- The special case concerning flow in the boundary layer behind a shock wave advancing into a fluid at rest leads to a result identical to those of references 2 and 8. This case is discussed in appendix B. The differential equations governing the boundary-layer flow in the centered expansion fan are found by substituting the free-stream relations of appendix A (equations (A1) to (A5) and (A7)) into equations (16) and (17) with the further qualification that

$$u_w = -a_\epsilon$$

$$\xi = 1 + \frac{\bar{x}}{a_\epsilon \bar{t}}$$

(19)

Results of this substitution are

$$\frac{C_w}{C_\epsilon}\left(1 - \frac{\gamma - 1}{\gamma + 1}\xi\right)^{\frac{3\gamma-1}{\gamma-1}} \frac{\partial^3 f}{\partial \eta^3} + \left(1 - \frac{\gamma - 1}{\gamma + 1}\xi\right)\left\{\frac{\partial^2 f}{\partial \eta^2}\left(\frac{\eta}{2} + \frac{3}{2}\frac{2}{\gamma + 1}\xi f + \right.\right.$$

$$\left.\frac{2}{\gamma + 1}\xi^2 \frac{\partial f}{\partial \xi}\right) + \left[(\xi - 1) - \frac{2}{\gamma + 1}\xi\frac{\partial f}{\partial \eta}\right]\left(\frac{\partial f}{\partial \eta} + \xi\frac{\partial^2 f}{\partial \eta \partial \xi}\right)\right\} +$$

$$\underline{h}_w + \left[(1 - \underline{h}_w) - 2\frac{\gamma - 1}{\gamma + 1}\xi + \left(\frac{\gamma - 1}{\gamma + 1}\right)^2\xi^2\right]g = 0$$

(20)

$$\frac{C_w}{C_\epsilon}\left(1 - \frac{\gamma - 1}{\gamma + 1}\xi\right)^{\frac{3\gamma-1}{\gamma-1}}\left\{\left[(1 - \underline{h}_w) - 2\frac{\gamma - 1}{\gamma + 1}\xi + \left(\frac{\gamma - 1}{\gamma + 1}\right)^2\xi^2\right]\frac{1}{N_{Pr}}\frac{\partial^2 g}{\partial \eta^2} + \right.$$

$$\left.(\gamma - 1)\left(\frac{2}{\gamma + 1}\right)^2\xi^2\left(\frac{\partial^2 f}{\partial \eta^2}\right)^2\right\} + \left(1 - \frac{\gamma - 1}{\gamma + 1}\xi\right)\left[(1 - \underline{h}_w) - 2\frac{\gamma - 1}{\gamma + 1}\xi + \right.$$

$$\left.\left(\frac{\gamma - 1}{\gamma + 1}\right)^2\xi^2\right]\left\{\frac{\partial g}{\partial \eta}\left(\frac{\eta}{2} + \frac{3}{2}\frac{2}{\gamma + 1}\xi f + \frac{2}{\gamma + 1}\xi^2\frac{\partial f}{\partial \xi}\right) + \xi\frac{\partial g}{\partial \xi}\left[(\xi - 1) - \frac{2}{\gamma + 1}\xi\frac{\partial f}{\partial \eta}\right]\right\} -$$

$$2\frac{\gamma - 1}{\gamma + 1}\xi\left(1 - \frac{\gamma - 1}{\gamma + 1}\xi\right)^2\left[(\xi - 1) - \frac{2}{\gamma + 1}\xi\frac{\partial f}{\partial \eta}\right]g + 2\frac{\gamma - 1}{\gamma + 1}\xi\left[(\xi - 1) - \right.$$

$$\left.\frac{2}{\gamma + 1}\xi\frac{\partial f}{\partial \eta}\right]\left\{\underline{h}_w + \left[(1 - \underline{h}_w) - 2\frac{\gamma - 1}{\gamma + 1}\xi + \left(\frac{\gamma - 1}{\gamma + 1}\right)^2\xi^2\right]g\right\} = 0$$

(21)

where

$$\frac{C_W}{C_\epsilon} = \left(\frac{T_W}{T_\epsilon}\right)^{0.5}\left(\frac{T_\epsilon + S}{T_W + S}\right)$$

The boundary conditions upon the functions f and g are the same as those given by equations (18).

Because of the complexity of these partial differential equations, solutions are sought in the form of infinite power series, which are written in powers of the conical coordinate ξ with the coefficients as functions of η only. Thus, the solutions are assumed as

$$\left.\begin{array}{l} f(\xi,\eta) = \displaystyle\sum_{n=0}^{\infty} \xi^n f_n(\eta) \\[4mm] g(\xi,\eta) = \displaystyle\sum_{n=0}^{\infty} \xi^n g_n(\eta) \end{array}\right\} \tag{22}$$

Because both of these partial differential equations possess singular points in the region $\xi \geq 1$ (see section entitled "Results and Discussion"), the infinite series can only represent the solutions in the region $\xi < 1$. The first few terms of each series are considered to approximate satisfactorily the exact solution in the region near the leading edge $\xi \ll 1$.

One further assumption is desirable. The enthalpy at the wall has already been assumed to be constant but arbitrary. The most common shock-tube physical arrangement dictates that the wall temperature before passage of the wave must be equal to the temperature of the undisturbed fluid. Thus, if the wall temperature is assumed to remain unchanged after passage of the wave because of the high thermal conductivity and heat capacity of metal walls, then

$$\left.\begin{array}{l} h_W = h_\epsilon \\[4mm] \dfrac{C_W}{C_\epsilon} = 1 \end{array}\right\} \tag{23}$$

Substitution of equations (22) and (23) into the equations of motion and energy (eqs. (20) and (21)), application of the boundary conditions (eqs. (18)), and equation of coefficients of like powers of ξ successively leads to an infinite set of ordinary linear differential equations and boundary conditions for each function, the first three of which are

$$f_0''' + \frac{\eta}{2}f_0'' - f_0' = -1 \tag{24a}$$

$$f_1''' + \frac{\eta}{2}f_1'' - 2f_1' = F_1(\eta) \tag{24b}$$

$$f_2''' + \frac{\eta}{2}f_2'' - 3f_2' = F_2(\eta) \tag{24c}$$

$$\left.\begin{array}{l} f_0(0) = f_0'(0) = 0 \\[2mm] f_0'(\infty) = 1 \end{array}\right\} \tag{25a}$$

$$f_n(0) = f_n'(0) = f_n'(\infty) = 0 \qquad \left(n \geqq 1\right) \tag{25b}$$

$$\frac{g_0''}{N_{Pr}} + \frac{\eta}{2}g_0' - g_0 = -1 \tag{26a}$$

$$\frac{g_1''}{N_{Pr}} + \frac{\eta}{2}g_1' - 2g_1 = G_1(\eta) \tag{26b}$$

$$\frac{g_2''}{N_{Pr}} + \frac{\eta}{2}g_2' - 3g_2 = G_2(\eta) \tag{26c}$$

$$\left.\begin{array}{l} g_0(0) = 0 \\[2mm] g_0(\infty) = 1 \end{array}\right\} \tag{27a}$$

$$g_n(0) = g_n(\infty) = 0 \qquad \left(n \geqq 1\right) \tag{27b}$$

with the following definitions:

$$F_1(\eta) = \frac{2\gamma}{\gamma + 1}f_0''' - \frac{3}{2}\frac{2}{\gamma + 1}f_0 f_0'' - f_0' + \frac{2}{\gamma + 1}(f_0')^2 + 2\frac{\gamma - 1}{\gamma + 1}g_0 - \frac{\gamma - 1}{\gamma + 1}$$

<div align="right">(28a)</div>

$$F_2(\eta) = \frac{2\gamma}{\gamma + 1}f_1''' - 2f_1' + 3\frac{2}{\gamma + 1}f_0'f_1' - \frac{3}{2}\frac{2}{\gamma + 1}f_0 f_1'' - \frac{5}{2}\frac{2}{\gamma + 1}f_1 f_0'' - $$

$$\frac{\gamma}{\gamma + 1}f_0''' + 2\frac{\gamma - 1}{\gamma + 1}g_1 + \left(\frac{\gamma - 1}{\gamma + 1}\right)^2(g_0 - 1)$$

<div align="right">(28b)</div>

$$G_1(\eta) = \frac{5}{2}\frac{\gamma - 1}{\gamma + 1}\frac{g_0''}{N_{Pr}} + \frac{\gamma - 5}{2(\gamma + 1)}\frac{\eta}{2}g_0' + \frac{2}{\gamma + 1}(f_0'')^2 - \frac{3}{2}\frac{2}{\gamma + 1}f_0 g_0' + $$

$$\frac{2}{\gamma + 1}f_0' g_0 - \frac{2}{\gamma + 1}f_0'$$

<div align="right">(28c)</div>

$$G_2(\eta) = \frac{2\gamma}{\gamma + 1}\frac{g_1''}{N_{Pr}} - \frac{\gamma + 7}{2(\gamma + 1)}g_1 - \frac{3}{2}\frac{2}{\gamma + 1}f_0 g_1' - \frac{5}{2}\frac{2}{\gamma + 1}f_1 g_0' + $$

$$2\frac{2}{\gamma + 1}f_0' g_1 + \frac{2}{\gamma + 1}f_1' g_0 - \frac{2}{\gamma + 1}f_1' + 2\frac{2}{\gamma + 1}f_0''f_1'' - $$

$$\frac{3\gamma^2 + 18\gamma - 13}{4(\gamma + 1)^2}\frac{g_0''}{N_{Pr}} + \frac{\gamma^2 - 14\gamma + 13}{4(\gamma + 1)^2}\frac{\eta}{2}g_0' - \frac{3}{2}\left(\frac{2}{\gamma + 1}\right)\left(\frac{\gamma - 1}{\gamma + 1}\right)f_0' - $$

$$\frac{1}{2}\frac{2}{\gamma + 1}\frac{3\gamma + 1}{\gamma + 1}(f_0'')^2 + \frac{3}{2}\frac{2}{\gamma + 1}\frac{\gamma - 1}{\gamma + 1}f_0' g_0$$

<div align="right">(28d)</div>

The primes on a symbol indicate differentiation with respect to the argument η.

Numerical integration of the preceding equations can be accomplished with no special difficulty. The momentum and energy equations for the nth functions are decoupled and hence may be solved independently. The particular integrals $F_n(\eta)$ and $G_n(\eta)$ are dependent only on previous solutions.

Equations (24) to (28) are solved for $f_n(\eta)$ and $g_n(\eta)$ and their respective derivatives, for $n = 0$, 1, and 2. These solutions then make possible approximation of the stream and enthalpy functions by the following relations which are valid in the vicinity of the leading edge:

$$f(\xi,\eta) \approx f_0(\eta) + \xi f_1(\eta) + \xi^2 f_2(\eta) \tag{29a}$$

$$g(\xi,\eta) \approx g_0(\eta) + \xi g_1(\eta) + \xi^2 g_2(\eta) \tag{29b}$$

Velocity and enthalpy profiles are given by

$$\frac{u}{u_1} = \frac{\partial f(\xi,\eta)}{\partial \eta} \approx f_0{}'(\eta) + \xi f_1{}'(\eta) + \xi^2 f_2{}'(\eta) \tag{30a}$$

$$\frac{h^*}{h_1{}^*} = \frac{h - h_w}{h_1 - h_w} = g(\xi,\eta) \approx g_0(\eta) + \xi g_1(\eta) + \xi^2 g_2(\eta) \tag{30b}$$

Skin Friction and Heat Transfer

The skin friction is given by

$$\tau_w = \left(\mu \frac{\partial u}{\partial y}\right)_{y=0} = \mu_w \left(\frac{\partial u}{\partial y}\right)_w \tag{31}$$

This relation is transformed to the $\xi,\eta,\bar{t}$ coordinate system through the transformation equations (9), (13), (14), and (15); the transformation yields the dimensionless friction

$$\hat{\tau}_w = \frac{\tau_w}{\rho_\epsilon a_\epsilon \sqrt{\dfrac{\nu_\epsilon}{\bar{t}}}} = \rho_1 \mu_1 C_w \frac{u_1}{\sqrt{\xi}} \left[\frac{\partial^2 f(\xi,\eta)}{\partial \eta^2}\right]_{\eta=0} \tag{32}$$

Finally, for the special case of expansion-fan boundary layer, from equations (23), it is seen that

$$\hat{\tau}_w = \underline{p}_1 \frac{u_1}{\sqrt{\xi}} \left[\frac{\partial^2 f(\xi,\eta)}{\partial \eta^2} \right]_{\eta=0} \tag{33}$$

where

$$\left[\frac{\partial^2 f(\xi,\eta)}{\partial \eta^2} \right]_{\eta=0} = f_0''(0) + \xi f_1''(0) + \xi^2 f_2''(0) \tag{33a}$$

The heat transferred per unit time per unit surface area from the wall to the fluid q_w is given by the relation

$$q_w = -k_w \left(\frac{\partial T}{\partial y} \right)_w \tag{34}$$

The transformation to the $\xi,\eta,\bar{t}$ system is accomplished in the same manner as for the skin friction and yields the dimensionless heat transfer

$$\hat{q}_w = \frac{q_w}{\rho_\epsilon a_\epsilon^2 \sqrt{\frac{\nu_\epsilon}{\bar{t}}}} = \frac{-\underline{p}_1 \mu_1 C_w}{N_{Pr}} \frac{1}{\sqrt{\xi}} \frac{h_1^*}{\gamma - 1} \left[\frac{\partial g(\xi,\eta)}{\partial \eta} \right]_{\eta=0} \tag{35}$$

The expansion-fan wall heat transfer is obtained from equation (35) and is

$$\hat{q}_w = -\frac{1}{N_{Pr}} \frac{\underline{p}_1}{\sqrt{\xi}} \frac{a_1^2 - 1}{\gamma - 1} \left[\frac{\partial g(\xi,\eta)}{\partial \eta} \right]_{\eta=0} \tag{36}$$

where

$$\left[\frac{\partial g(\xi,\eta)}{\partial \eta} \right]_{\eta=0} = g_0'(0) + \xi g_1'(0) + \xi^2 g_2'(0) \tag{36a}$$

Transformation to the Physical Plane

The transformation to the physical coordinate system is carried out by using the profile functions. The incompressible normal coordinate Y was defined by equations (9). The reverse transformation is

$$y = \int_0^Y \frac{\rho_\epsilon}{\rho(\bar{x},Y,\bar{t})}\, dY = \frac{1}{\underline{p}_1(\bar{x},\bar{t})} \int_0^Y \frac{h(\bar{x},Y,\bar{t})}{h_\epsilon}\, dY \qquad (37)$$

Since the local enthalpy is given as a function of ξ and η by equation (30b), the integration of equation (37) is most easily accomplished in those coordinates. The transformation equations defining ξ and η (eqs. (15)) are used to define the differential dY as

$$dY = \sqrt{\nu_\epsilon \xi \bar{t}}\left(d\eta + \frac{\eta}{2}\frac{d\bar{t}}{\bar{t}} + \frac{\eta}{2}\frac{d\xi}{\xi}\right) \qquad (38)$$

The integration (eq. (37)) is to be carried out at constant $\bar{x}$ and $\bar{t}$ and thus at constant ξ and $\bar{t}$; as a result of combining equations (38) and (37), the physical normal coordinate y is

$$y = \frac{\sqrt{\nu_\epsilon \xi \bar{t}}}{\underline{p}_1} \int_0^\eta \frac{h(\xi,\eta,\bar{t})}{h_\epsilon}\, d\eta \qquad (39)$$

Substitution of the enthalpy function from equation (30b), rearrangement of the terms, replacement of $\bar{t}$ by its equivalent t, and integration of equation (39) yields for $h_w = h_\epsilon$:

$$\frac{y}{\sqrt{\nu_\epsilon \xi t}} = \frac{1}{\underline{p}_1}\eta + \frac{\underline{h}_1{}^*}{\underline{p}_1}\left[\int_0^\eta g_0(\eta)d\eta + \xi \int_0^\eta g_1(\eta)d\eta + \xi^2 \int_0^\eta g_2(\eta)d\eta\right] \qquad (40)$$

The quantity $\dfrac{y}{\sqrt{\nu_\epsilon \xi\, t}}$ is the physical compressible counterpart of the incompressible similarity parameter η and is a function only of ξ and η.

RESULTS AND DISCUSSION

Numerical Results

Each of the homogeneous differential equations corresponding to the complete equations (24) and (26) was transformed to Hermite's differential equation and complementary solutions in the form of Hermite polynomials were obtained. (See ref. 14.) Except for the $n = 0$ case, particular solutions appeared to be unobtainable in closed form. Rather than combine the Hermite polynomials with particular integrals found by numerical procedures, it was decided to treat by numerical methods the complete equations for the cases $n \geq 1$.

In reference 15, the laminar boundary layer on a flat plate uniformly accelerated from rest was investigated. The resulting momentum equation and boundary conditions for the initial motion of the plate are equivalent to those of the present analysis for $n = 0$ (eqs. (24a) and (25a)) and the complete solution (from ref. 15) is therefore

$$f_0(\eta) = \frac{2}{\sqrt{\pi}}\left[1 - e^{-\left(\frac{\eta}{2}\right)^2}\right] - \frac{\eta^3}{6} + \int_0^\eta \left(\frac{\varphi^2 + 2}{\sqrt{\pi}} \int_0^{\varphi/2} e^{-\theta^2} d\theta\right) d\varphi \qquad (41)$$

$$f_0'(\eta) = -\frac{\eta^2}{2} + \frac{\eta}{\sqrt{\pi}} e^{-(\eta/2)^2} + \frac{\eta^2 + 2}{\sqrt{\pi}} \int_0^{\eta/2} e^{-\theta^2} d\theta \qquad (42)$$

It can be shown that the first term on the right-hand side of equation (42) is the particular integral and the two remaining terms are the exponential form of the appropriate Hermite polynomial, the complementary solution.

The energy differential equation is of the same form as the momentum equation, and the following solution may be deduced:

$$g_0(\eta) = -N_{Pr} \frac{\eta^2}{2} + \frac{\eta\sqrt{N_{Pr}}}{\sqrt{\pi}} e^{-N_{Pr}(\eta/2)^2} + \frac{N_{Pr}\eta^2 + 2}{\sqrt{\pi}} \int_0^{\sqrt{N_{Pr}}\,\eta/2} e^{-\theta^2} d\theta \qquad (43)$$

These functions satisfy the respective boundary conditions and are given in table I for N_{Pr} equal to 0.72.

Numerical integration of the higher order differential equations was carried out on the Bell Telephone Laboratories X-66744 relay computer at the Langley Laboratory by using a modification of the Runge-Kutta fourth-order method given in reference 16. (The ratio of specific heats γ was set equal to 1.4.) Results of these computations are listed in tables II and III. The functions most important to the analysis are $f_n'(\eta)$ and $g_n(\eta)$, the nth order velocity and enthalpy profiles, respectively; plots of these functions are given in figure 3.

The actual velocity and enthalpy profiles in the $\xi, \eta, \bar{t}$ coordinate system are approximated by equations (30a) and (30b) and have been computed for values of ξ equal to 0, 0.1, 0.2, 0.3, and 0.5. The results of this computation are shown in figure 4. Since the power series for both velocity and enthalpy profiles neglect terms of order ξ^3, the results are considered to be quantitatively correct only in the range $0 \leqq \xi \leqq 0.3$. Extension of the results up to $\xi = 0.5$ is included for qualitative indication of trends. Skin-friction and heat-transfer functions are shown in figure 5 with three approximate formulas for each, corresponding to taking one, two, or three terms of the power series.

The transformation integrals were computed by graphical integration of the appropriate functions given in tables I to III, and are listed in table IV. The function defined by equation (40) is computed for values of ξ of 0, 0.1, 0.2, 0.3, and 0.5, and the results are plotted in figure 6. Theoretical velocity and enthalpy difference profiles in the physical x, y, t coordinate system have been computed and are given in figure 7 for values of ξ of 0.1, 0.2, 0.3, and 0.5 with the infinite series approximated by the three term series. The normal coordinate parameter $y/\sqrt{\nu_\epsilon t}$ is used in place of $y/\sqrt{\nu_\epsilon \xi t}$ so that adjacent profiles may be more easily distinguished.

Discussion of Results

As mentioned previously, the zero-order momentum equation for the present case was found to be identical to that of reference 15, the initial motion of a flat plate uniformly accelerated from rest. This result is not surprising in view of the fact that the present case may be considered to be a form of constant acceleration; that is, the potential-flow velocity varies linearly with the conical coordinate ξ. The respective coordinates of the reference are also closely related to the coordinates ξ and η used herein.

Figures 4 and 7 are apparently contradictory; figures 4(a) and 4(b) show profiles becoming increasingly full as ξ is increased whereas the corresponding plots of figures 7(a) and 7(b) indicate velocity and enthalpy difference profiles behaving in the opposite manner. This

condition is the effect of distortion of the normal coordinate by plotting
it in the incompressible η-plane as opposed to plotting it in the physical
$y\big/\sqrt{\nu_\epsilon t}$-plane, and no contradiction actually exists.

For ξ equal to 0.5, both velocity and enthalpy difference profiles
in figures 4 and 7 show a slight tendency to oscillate once near the free-
stream boundary, the latter profile actually exceeding a value of unity
inside the boundary layer. The trend indicates that the velocity also
will exceed unity within the boundary layer for values of ξ larger
than 0.5. Because the amplitude of oscillation is extremely small and
the estimated error of the present solution for the three-term-series
approximation is of the order of ξ^3, these results are open to question.
However, velocity profiles exceeding unity have been encountered in
steady-flow theories under conditions of a strong favorable stream pres-
sure gradient and high ratio of wall temperature to stream temperature
(ref. 17); such stream and wall conditions are present near the leading
edge of the expansion fan. Thus, although these profiles must be ques-
tioned in view of the limits of validity of the present series solutions,
the velocity profile, at least, is typical of certain steady-flow velocity
profiles in fluid undergoing similar processes.

The heat transfer given by the three-term-series approximation
(fig. 5(b)) apparently reaches a maximum at $\xi \approx 0.4$ and then decreases.
This result may be qualitatively explained by considering the difference
between the wall enthalpy and the stream stagnation enthalpy, which
forms a sort of heat-transfer potential. The stream stagnation enthalpy
$h_{o,1}$ is derived from the expansion-fan relations of appendix A and is
given by

$$\underline{h}_{o,1} = \frac{h_{o,1}}{h_\epsilon} = \frac{h_1}{h_\epsilon} + \frac{u_1^2}{2h_\epsilon} = 1 + \frac{\gamma - 1}{\gamma + 1}\left(\xi^2 - 2\xi\right) \qquad (44)$$

The dimensionless potential, $\underline{h}_w - \underline{h}_{o,1}$ for the case $h_w = h_\epsilon$, is
plotted in figure 8. The rate of heat transfer follows the same general
trend as the total enthalpy difference for an increase in the conical
coordinate near the leading edge.

If this line of reasoning is followed, one might expect that, in the
region where the stagnation enthalpy difference becomes very strongly
negative, the rate of heat transfer might also become negative and would
thus indicate heat transfer from the fluid to the wall. This is indeed
the case with the integral solution of reference 12 where the heat-
transfer function goes from positive to negative at a value of the conical
coordinate $\xi \approx 1.5$. The present solution cannot be carried to that

extent, but examination of the enthalpy function of the second power of ξ ($g_2(\eta)$ in fig. 3(b)) indicates a reversal of sign in the derivatives at the wall ($\eta = 0$); thus, a tendency for the heat transfer to reverse is shown. This term in the power series increases in importance with increasing ξ and lends support to the belief that regions of negative rates of heat transfer (from fluid to wall) exist beyond the region of validity of the present solution.

Comparison With Solution of Zero-Thickness Expansion Wave

Reference 9 considers the expansion fan as a wave of zero thickness propagating into fluid at rest at a velocity equal to $-a_\epsilon$. The wave diagram for the special case of shock-tube flow under this assumption is shown in figure 9(a); the true fan is illustrated in figure 9(b). The zero thickness wave coincides with the line $\xi = 0$. Isentropic expansion-fan relations are assumed to hold across the zero-thickness wave, and the entire region from the wave to the temperature discontinuity is assumed to be a region of constant stream properties and corresponds to region α in the true shock-tube case. Comparison of the results of the present analysis with those of reference 9 is carried out on the basis of equal potential flows. That is, if the value of ξ at the trailing edge of the expansion fan ξ_{te} is given, free-stream variables in the constant potential flow region α $\left(\text{that is } p_\alpha, u_\alpha, \text{ and so forth}\right)$ may be found from appendix A (eqs. (A1) to (A5) evaluated at ξ_{te}). These variables are also the free-stream variables for the corresponding zero-thickness expansion-wave solution. Since the present analysis does not consider the region $\xi > \xi_{te}$ (region α), comparison must be restricted to the region $0 \leqq \xi \leqq \xi_{te}$ for each case, although the results of reference 9 are extended beyond this region in figure 10. The asterisks appearing on the curves represent the appropriate positions of ξ_{te}.

Skin-friction and heat-transfer functions are shown in figure 10 for ξ_{te} equal to 0.1, 0.2, 0.3, and 0.5, the present solution corresponding to the three-term (quadratic) power-series approximations (eqs. (33a) and (36a)). It is apparent that the two solutions are very different; the skin friction and heat transfer for each zero-thickness expansion solution approach infinity at the wave $\xi = 0$, whereas the corresponding functions for the expansion fan vanish. One might consider this behavior analogous with that of a flat plate and of a blunt body in steady flow. Skin friction and heat transfer at the leading edge of a flat plate are infinite whereas, at the forward stagnation point of a blunt body, friction vanishes and heat transfer is finite, depending upon wall temperature. Whether these discrepancies are important in computing shock attenuation, however, will depend upon the strength of the wave in question. For weak waves, although the details of the flow within the narrow fan have been shown to be very different, effects upon shock attenuation may be small as they

represent integrated wall shear and heat transfer far downstream. Here
the steady-flow analogy is with the flow well downstream of the leading
edges of the flat plate and the blunt body where the leading edge is not
important. For strong waves, however, the flow within the fan may
seriously influence the shock wave. It should be pointed out that
although the computations of reference 9 were carried out for strong as
well as weak expansions, the limitations of the analysis were therein
recognized.

It is of interest to note that, at $\xi = \xi_{te}$ in the zero-thickness-
wave case, the skin-friction and heat-transfer functions are approximately
one-half the corresponding expansion-fan values. This relation is more
evident if skin-friction and heat-transfer coefficients defined by

$$\bar{\tau}_w = \frac{\tau_w}{\rho_w u_1 \sqrt{\dfrac{\nu_\epsilon}{\bar{t}\xi}}} \tag{45}$$

$$\bar{q}_w = \frac{q_w}{\rho_w \dfrac{h_1{}^*}{N_{Pr}} \sqrt{\dfrac{\nu_\epsilon}{\bar{t}\xi}}} \tag{46}$$

are considered. For the present solution, combination of equations (33)
and (45) and of (36) and (46) yields, respectively,

$$\bar{\tau}_w = \left(\frac{\partial^2 f(\xi,\eta)}{\partial \eta^2}\right)_{\eta=0} \tag{47}$$

$$\bar{q}_w = \left(\frac{\partial g(\xi,\eta)}{\partial \eta}\right)_{\eta=0} \tag{48}$$

The corresponding coefficient form from reference 9 is independent of
coordinate ξ and is a function only of expansion strength ξ_{te}. These
coefficients are shown in figure 11; the values from reference 9 are
approximately one-half those of the present solution. This relation is
exact for the limit $\xi_{te} = 0$ (an infinitesimally weak wave) where the
following values apply:

	Present solution	Reference 9
$\bar{\tau}_w$	$2\sqrt{\dfrac{1}{\pi}}$	$\sqrt{\dfrac{1}{\pi}}$
$\bar{q}_w$	$2\sqrt{\dfrac{N_{Pr}}{\pi}}$	$\sqrt{\dfrac{N_{Pr}}{\pi}}$

The zero-thickness-wave case is discussed further in appendix B. A more detailed comparison of the finite-width and zero-thickness expansion waves is made in reference 12.

Singularities in the Flow Field

The equations of momentum and energy were transformed to the $\xi,\eta,\bar{t}$ coordinate system (eqs. (16) and (17)) and then specialized for the case of the centered expansion-fan potential flow (eqs. (20) and (21)). It is of interest to note that the aforementioned equations indicate mathematical singularities in the flow field. This condition can be observed in the expression

$$\left[(\xi - 1) - u_1 \frac{\partial f}{\partial \eta}\right] = \left[(\xi - 1) - \frac{2}{\gamma + 1}\xi\frac{\partial f}{\partial \eta}\right] \qquad (49)$$

which is the coefficient of the highest order derivative with respect to ξ in each of the partial differential equations. For $1 \leqq \xi \leqq 1 + u_1$, this term vanishes somewhere in the boundary layer and, as a result, the solution became nonanalytic (that is, a singular point). In the x,y,t coordinate system, the singularity occurs at a position

$$\left(\frac{x}{a_\epsilon t}\right)_{\text{singularity}} = u_1 \frac{\partial f}{\partial \eta} = u(x,y,t)$$

It is evident, since u is always positive (in the positive x-direction), that the singularity always appears in the region $x \geqq 0$ and is actually within the limits $0 \leqq \frac{x}{a_\epsilon t} \leqq u_1$.

The appearance of these singularities is discussed in reference 18 in regard to the impulsive motion of a semi-infinite flat plate in an

incompressible fluid. David Adamson has made an independent investigation
of this case at the Langley Laboratory and he argues that, although the
vorticity generated at the plate surface at the start of motion diffuses
normal to the surface at an infinite rate, the Prandtl boundary-layer
assumptions allow no diffusion of vorticity in the streamwise direction.
At the origin of motion, the flow field of this case consists of the
undisturbed fluid ahead of the leading edge, and the fluid behind the
leading edge through which the vorticity of starting has already spread
in a direction normal to the surface. A line singularity separates these
regions and, as time progresses, this singularity is swept downstream.

The singularities in the expansion fan may be considered in an analo-
gous fashion as originating at the point $x = t = 0$ (the diaphragm sta-
tion at burst in shock-tube flow, for example) with vorticity generated at
this point and diffused immediately only in the normal y-direction. As
time progresses, the singularity is swept downstream (in the positive
x-direction). When the expansion fan is supersonic ($\xi_{te} > 1$), these
singularities appear in the fan itself; thus, the present series solu-
tion is limited as already discussed.

The singularities exist, however, even when the expansion fan is sub-
sonic, that is, $\xi_{te} < 1$. The condition of a nonanalytic solution must
still occur in the region where $\xi \geqq 1$ even though this region may be down-
stream of the expansion-fan trailing edge because the physical reasoning
describing the diffusion of vorticity is qualitatively independent of
expansion-fan strength. As a result, one would expect the analysis based
upon a zero-thickness expansion wave to exhibit singular behavior in the
region $\xi \geqq 1$. The fact that no such behavior was evident in the data of
reference 9 is attributed to the fact that the origin of the wave (for
example, the diaphragm burst) was neglected therein when the flow was
assumed to be steady with respect to a coordinate system fixed to the wave.
The zero-thickness wave, as applied to the shock tube in references 6 and
10, therefore implied a wave which originated at $t = -\infty$, propogated at
a constant velocity equal to $-a_\epsilon$, and passed through the point $x = t = 0$
on the x,t diagram (fig. 12). Consideration of the zero-thickness expan-
sion wave by the present method (see appendix B) does result in the
expected mathematical singularities.

CONCLUDING REMARKS

A solution to the laminar boundary-layer equations that is valid near
the leading edge of an expansion wave of finite width has been obtained.
Application of the results to the calculation of real gas flow in a shock
tube by the method of NACA Technical Note 3375 involves the use of the
skin-friction and heat-transfer results along with like functions appro-
priate to the cold-gas constant-potential-flow region. The present

solution could also be adapted for application to the method of NACA Technical Note 3278 by computation of the velocity normal to the wall. For this application, solutions in the region between the fan trailing edge and the temperature discontinuity, including the associated singularities, also would be required.

The zero-thickness expansion-wave solution of NACA Technical Note 3712 indicates the skin-friction and heat-transfer results to be very different from those obtained herein. In principle, then, substitution of a zero-thickness wave for a true expansion fan in computing the boundary layer must be questioned both on grounds of accuracy near the leading edge and of omission from the consideration of the singularities in the flow field in the region downstream of the position of the origin of the wave. In application to the shock-tube case, however, the results of NACA Technical Note 3278 indicate that the hot gas compressed by the shock is the primary factor influencing shock-wave attenuation for moderate pressure ratios; thus, in practice, assumption of a zero-thickness expansion wave may not seriously affect the theoretical attenuation results.

No experimental boundary-layer data for laminar flow in a centered expansion fan are available. Local heat-transfer rates within the fan can be measured, and such measurements may substantiate the present theory. Data on shock-wave attenuation are plentiful, but little information regarding the fan may be deduced since the effects of the shock-compressed gas generally predominate and flow Reynolds numbers are frequently in the turbulent range. Future application of the integral solution to turbulent boundary layers should afford both direct and indirect checks on that theory and should lead to more definite conclusions regarding the present theory.

Langley Aeronautical Laboratory,
    National Advisory Committee for Aeronautics,
        Langley Field, Va., December 3, 1956.

APPENDIX A

FREE-STREAM RELATIONS IN THE EXPANSION FAN

The equations defining the flow parameters of a fluid undergoing acceleration in a centered expansion fan are listed, for example, in reference 1 to 3 and are reproduced below in terms of the coordinate $\xi = \frac{x}{a_\epsilon t} + 1$:

$$\underline{u}_1 = \frac{2}{\gamma + 1}\xi \tag{A1}$$

$$\underline{a}_1 = 1 - \frac{\gamma - 1}{\gamma + 1}\xi \tag{A2}$$

$$\underline{h}_1 = \left(\underline{a}_1\right)^2 \tag{A3}$$

$$\underline{p}_1 = \left(\underline{a}_1\right)^{\frac{2\gamma}{\gamma-1}} \tag{A4}$$

$$\underline{\rho}_1 = \left(\underline{a}_1\right)^{\frac{2}{\gamma-1}} \tag{A5}$$

The stream viscosity is written by using the Sutherland relation as

$$\underline{\mu}_1 = \frac{\mu_1}{\mu_\epsilon} = \left(\frac{T_1}{T_\epsilon}\right)^{1.5}\left(\frac{T_\epsilon + S}{T_1 + S}\right) \tag{A6}$$

Equation (A6) is combined with the equation of state (eq. (4)) and the definition of C_w (eq. (8)); from the resulting relation are obtained the viscosity terms in the differential equations of motion and energy

$$\underline{\rho}_1\underline{\mu}_1 C_w = \underline{p}_1 \frac{C_w}{C_\epsilon} \tag{A7}$$

where

$$\frac{1}{C_\epsilon} = \left(\frac{T_1}{T_\epsilon}\right)^{0.5}\left(\frac{T_\epsilon + S}{T_1 + S}\right) \tag{A8}$$

Equations (8) and (A8) may be combined to yield

$$\frac{C_w}{C_\epsilon} = \left(\frac{T_w}{T_\epsilon}\right)^{0.5}\left(\frac{T_\epsilon + S}{T_w + S}\right) \tag{A9}$$

For the special case $T_w = T_\epsilon$, it is seen that

$$\frac{C_w}{C_\epsilon} = 1 \tag{A10}$$

APPENDIX B

BOUNDARY LAYER BEHIND SHOCK OR ZERO-THICKNESS

EXPANSION WAVE MOVING INTO FLUID AT REST

The flow behind a shock wave or a zero-thickness expansion wave may be considered by utilizing the theory of this paper modified for constant potential flow. The x,t diagram of figure 9(a) shows both cases. Although the shock wave advances into the low-pressure region ∞, region ε remains the reference for both solutions. The wave velocity u_W is equal to u_s in the shock-wave case and is equal to $-a_ε$ in the zero-thickness expansion-wave case.

The following relations result from the equations of motion and energy (eqs. (16) and (17)) for constant potential flow:

$$\rho_1 \mu_1 C_w \frac{u_1}{\xi} \frac{\partial^3 f}{\partial \eta^3} + \frac{\partial^2 f}{\partial \eta^2}\left[\frac{u_1}{2\xi}\eta - \frac{u_1}{u_W}\left(\frac{u_1}{2\xi}f + u_1 \frac{\partial f}{\partial \xi}\right)\right] + \left[(\xi - 1) + \frac{u_1}{u_W}\frac{\partial f}{\partial \eta}\right]u_1 \frac{\partial^2 f}{\partial \eta \partial \xi} = 0$$

$$\text{(B1)}$$

$$\rho_1 \mu_1 C_w\left[\frac{1}{N_{Pr}}\frac{h_1^*}{\xi}\frac{\partial^2 g}{\partial \eta^2} + (\gamma - 1)\frac{u_1^2}{\xi}\left(\frac{\partial^2 f}{\partial \eta^2}\right)^2\right] + h_1^* \frac{\partial g}{\partial \eta}\left[\frac{\eta}{2\xi} - \frac{u_1}{u_W}\left(\frac{1}{2\xi}f + \frac{\partial f}{\partial \xi}\right)\right] +$$

$$h_1^* \frac{\partial g}{\partial \xi}\left[(\xi - 1) + \frac{u_1}{u_W}\frac{\partial f}{\partial \eta}\right] = 0 \qquad\qquad \text{(B2)}$$

Boundary conditions are the same as those given by equations (18) and the coordinates ξ and η are defined in equations (15); these values are valid for both cases under consideration. Note that ξ is zero on the wave in each case. Solutions in the following regions are desired (see fig. 9(a)):

(a) Shock-wave case; region β

$$0 \leqq \xi = 1 - \frac{\bar{x}}{u_s \bar{t}} \leqq \left(1 - \frac{u_1}{u_s}\right)$$

(b) Zero-thickness expansion case; region α

$$0 \leqq \xi = 1 + \frac{\bar{x}}{a_\epsilon \bar{t}} \leqq \left(1 + \underline{u}_1\right)$$

Note also that

$$\left(u_1\right)_\alpha = \left(u_1\right)_\beta$$

and that, in general,

$$\left(h_1\right)_\alpha \neq \left(h_1\right)_\beta$$

Direct solutions of equations (B1) and (B2) appear unlikely. The coefficient of the leading partial derivative with respect to ξ in equations (B1) and (B2) is given by

$$\left[(\xi - 1) + \frac{\underline{u}_1}{\underline{u}_w} \frac{\partial f}{\partial \eta}\right] = \left[(\xi - 1) + \frac{u}{\underline{u}_w}\right]$$

and the vanishing of this coefficient introduces singularities into the flow field at positions given by

$$1 \geqq \xi \geqq 1 - \frac{\underline{u}_1}{\underline{u}_s}$$

or

$$0 \leqq \frac{x}{u_s t} \leqq \frac{\underline{u}_1}{\underline{u}_s}$$

for the flow behind a shock, and

$$1 \geqq \xi \geqq 1 + \underline{u}_1$$

or

$$0 \leqq \frac{x}{a_\epsilon t} \leqq \underline{u}_1$$

for the case of flow behind a zero-thickness expansion fan.

Power-series solutions are assumed, as in the expansion-fan case, and are given by

$$f(\xi,\eta) = \sum_{n=0}^{\infty} \xi^n f_n(\eta) \qquad \qquad \text{(B3)}$$

$$g(\xi,\eta) = \sum_{n=0}^{\infty} \xi^n g_n(\eta) \qquad \qquad \text{(B4)}$$

Because of the location of the singularities, it is apparent that this power series is valid only in the following regions:

Shock-wave case:

$$0 \leqq \xi < 1 - \frac{\underline{u}_1}{\underline{u}_s}$$

Expansion-wave case:

$$0 \leqq \xi < 1$$

For the flow behind the shock, this region is precisely the region β; hence the series solution is sufficient. The region of validity of the series solution for the expansion-wave case is only part of the cold-gas region α, and it is in this region that the series solution will be inadequate.

Equations (B3) and (B4) are substituted into equations (B1) and (B2); after expanding and collecting terms, coefficients of like powers of ξ are equated. The first three equations of each set and the corresponding boundary conditions are

$$\underline{\rho_1}\underline{\mu_1}C_w f_0''' + \frac{\eta}{2}f_0'' - \frac{1}{2}\frac{u_1}{u_w}f_0 f_0'' = 0 \tag{B5a}$$

$$\underline{\rho_1}\underline{\mu_1}C_w f_1''' + \left(\frac{\eta}{2} - \frac{1}{2}\frac{u_1}{u_w}f_0\right)f_1'' - \left(1 - \frac{u_1}{u_w}f_0'\right)f_1' - \frac{3}{2}\frac{u_1}{u_w}f_1 f_0'' = 0 \tag{B5b}$$

$$\underline{\rho_1}\underline{\mu_1}C_w f_2''' + \left(\frac{\eta}{2} - \frac{1}{2}\frac{u_1}{u_w}f_0\right)f_2'' - \left(1 - \frac{u_1}{u_w}f_0'\right)2f_2' - \frac{5}{2}\frac{u_1}{u_w}f_0''f_2 -$$

$$\frac{3}{2}\frac{u_1}{u_w}f_1 f_1'' + \left(1 + \frac{u_1}{u_w}f_1'\right)f_1' = 0 \tag{B5c}$$

$$\left.\begin{array}{l} f_0(0) = 0 \\[4pt] f_0'(0) = 0 \\[4pt] f_0'(\infty) = 1 \end{array}\right\} \tag{B6a}$$

$$f_n(0) = f_n'(0) = f_n'(\infty) = 0 \qquad \left(n \geqq 1\right) \tag{B6b}$$

$$\underline{\rho_1}\underline{\mu_1}C_w\left[\frac{g_0''}{N_{Pr}} + (\gamma - 1)\frac{u_1^2}{\underline{h_1}^*}f_0''^2\right] + \frac{\eta}{2}g_0' - \frac{1}{2}\frac{u_1}{u_w}f_0 g_0' = 0 \tag{B7a}$$

$$\underline{\rho_1}\underline{\mu_1}C_w\left[\frac{g_1''}{N_{Pr}} + 2(\gamma - 1)\frac{u_1^2}{\underline{h_1}^*}f_0''f_1''\right] + \left(\frac{\eta}{2} - \frac{1}{2}\frac{u_1}{u_w}f_0\right)g_1' -$$

$$\left(1 - \frac{u_1}{u_w}f_0'\right)g_1 - \frac{3}{2}\frac{u_1}{u_w}f_1 g_0' = 0 \tag{B7b}$$

$$\underline{\rho_1}\underline{\mu_1}C_w\left[\frac{g_2''}{N_{Pr}} + \left(f_1''^2 + 2f_0''f_2''\right)(\gamma - 1)\frac{u_1^2}{\underline{h_1}^*}\right] + \left(\frac{\eta}{2} - \frac{1}{2}\frac{u_1}{u_w}f_0\right)g_2' -$$

$$2\left(1 - \frac{u_1}{u_w}f_0'\right)g_2 - \frac{3}{2}\frac{u_1}{u_w}f_1 g_1' + \left(1 + \frac{u_1}{u_w}f_1'\right)g_1 - \frac{5}{2}\frac{u_1}{u_w}f_2 g_0' = 0 \tag{B7c}$$

$$g_0(0) = 0 \left.\right\}$$
$$g_0(\infty) = 1 \left.\right\} \qquad\qquad\qquad (B8a)$$

$$g_n(0) = g_n(\infty) = 0 \qquad \left(n \geqq 1\right) \qquad (B8b)$$

Equations (B5a) and (B7a) for f_0 and g_0 may be integrated numerically. Solutions of the remaining equations are

$$f_1(\eta) = f_2(\eta) = \ldots = 0 \left.\right\}$$
$$g_1(\eta) = g_2(\eta) = \ldots = 0 \left.\right\} \qquad\qquad (B9)$$

Thus, both infinite-series representations of the functions reduce to the simple relations

$$f(\xi,\eta) = f_0(\eta) \left.\right\}$$
$$g(\xi,\eta) = g_0(\eta) \left.\right\} \qquad\qquad\qquad (B10)$$

For constant potential flow, the similar stream and enthalpy functions are functions of η only, a result which could have been obtained directly by modifying the similarity transformations (eqs. (13) and (14)).

Equations (B5a) and (B7a) and the appropriate boundary conditions may be transformed into equations (9) and (10) of reference 9 for both shock and zero-thickness expansion waves if the special case $h_w = h_\epsilon$ is considered. For this reason, no attempt to evaluate the constant-potential-flow solutions is made herein. Singularities apparent in the present solution, however, were not evident in reference 9. These singularities represent vorticity, generated by the start of motion at $t = 0$, which diffused normal to the wall at an infinite rate and then was washed downstream. By considering both problems as independent of time when treated in a coordinate system fixed to the wave, reference 9 neglected the start of motion and hence, in the shock-tube case, implied a wave which originated at $t = -\infty$, propagated through the point $x = t = 0$, and continued on. In this case singularities were thus not evident.

Figure (12) shows the location of the singularities. When the flow behind the shock wave is considered, only region β is of interest; thus,

the singularities existing outside this region do not affect the solu-
tion. Only flow behind the zero thickness expansion wave involves
singular behavior within the region of interest, and this phenomenon
should, in principle, be considered in computing shock-tube boundary
layer. The expansion-wave solution of reference 9 then is actually
valid only in the region $0 \leqq \xi < 1$.

REFERENCES

1. Glass, I. I., Martin, W., and Patterson, G. N.: A Theoretical and Experimental Study of the Shock Tube. UTIA Rep. No. 2, Inst. of Aerophysics, Univ. of Toronto, Nov. 1953.

2. Hollyer, Robert N., Jr.: A Study of Attenuation in the Shock Tube. Proj. M720-4 (Contract N6-ONR-232-TO IV, Office of Naval Res.), Univ. of Michigan Eng. Res. Inst., July 1, 1953.

3. Huber, Paul W., Fitton, Cliff E., Jr., and Delpino, F.: Experimental Investigation of Moving Pressure Disturbances and Shock Waves and Correlation With One-Dimensional Unsteady-Flow Theory. NACA TN 1903, 1949.

4. Donaldson, Coleman duP., and Sullivan, Roger D.: The Effect of Wall Friction on the Strength of Shock Waves in Tubes and Hydraulic Jumps in Channels. NACA TN 1942, 1949.

5. Emrich, R. J., and Curtis, C. W.: Attenuation in the Shock Tube. Jour. Appl. Phys., vol. 24, no. 3, Mar. 1953, pp. 360-363.

6. Trimpi, Robert L., and Cohen, Nathaniel B.: A Theory for Predicting the Flow of Real Gases in Shock Tubes With Experimental Verification. NACA TN 3375, 1955.

7. Mack, John E.: Density Measurement in Shock Tube Flow With the Chrono-Interferometer. Tech. Rep. 4, Lehigh Univ. Inst. Res. (Proj. NR 061-063, Contract N7onr39302, Office of Naval Res.), Apr. 15, 1954.

8. Mirels, Harold: Laminar Boundary Layer Behind Shock Advancing Into Stationary Fluid. NACA TN 3401, 1955.

9. Mirels, Harold: Boundary Layer Behind Shock or Thin Expansion Wave Moving Into Stationary Fluid. NACA TN 3712, 1956.

10. Mirels, Harold: Attenuation in a Shock Tube Due to Unsteady-Boundary-Layer Action. NACA TN 3278, 1956.

11. Williams, Albert Charles: Propagation of the Effects of Wall Interaction in the Rarefaction Region of Shock Tube Flow. Tech. Rep. 6, Inst. of Research, Lehigh Univ. (Project NR 061-063, Contract N7onr39302, Office of Naval Res.), Aug. 15, 1955.

12. Trimpi, Robert L., and Cohen, Nathaniel B.: An Integral Solution to the Flat-Plate Laminar Boundary-Layer Flow Existing Inside and After Expansion Waves and After Shock Waves Moving into Quiescent Fluid With Particular Application to the Complete Shock-Tube Flow. NACA TN 3944, 1957.

13. Chapman, Dean R., and Rubesin, Morris W.: Temperature and Velocity
    Profiles in the Compressible Laminar Boundary Layer With Arbitrary
    Distribution of Surface Temperature. Jour. Aero. Sci., vol. 16,
    no. 9, Sept. 1949, pp. 547-565.

14. Margenau, Henry, and Murphy, George Moseley: The Mathematics of
    Physics and Chemistry. D. Van Nostrand Co., Inc., 1943.

15. Moore, Franklin K.: Unsteady Laminar Boundary-Layer Flow. NACA
    TN 2471, 1951

16. Gill, S.: A Process for the Step-by-Step Integration of Differential
    Equations in an Automatic Digital Computing Machine. Proc. Cambridge
    Phil. Soc., vol. 47, pt. 1, Jan. 1951, pp. 96-108.

17. Brown, W. Byron, and Donoughe, Patrick L.: Tables of Exact Laminar-
    Boundary-Layer Solutions When the Wall Is Porous and Fluid Properties
    Are Variable. NACA TN 2479, 1951.

18. Stewartson, K.: On the Impulsive Motion of a Flat Plate in a Viscous
    Fluid. Quarterly Jour. Mech. and Appl. Math., vol. IV, pt 2, June
    1951, pp. 182-198.

TABLE I.- VELOCITY AND ENTHALPY FUNCTIONS, $n = 0$ TERMS

$$\left[N_{Pr} = 0.72\right]$$

η	f_0	f_0'	f_0''	g_0	g_0''
0	0	0	1.1284	0	0.9575
.20	.0213	.2064	.9396	.1775	.8203
.40	.0802	.3773	.7732	.3290	.6969
.60	.1702	.5172	.6284	.4572	.5868
.80	.2854	.6301	.5043	.5646	.4897
1.00	.4208	.7201	.3993	.6539	.4048
1.20	.5722	.7910	.3119	.7273	.3314
1.40	.7362	.8459	.2402	.7872	.2687
1.60	.9098	.8880	.1823	.8355	.2157
1.80	1.0908	.9197	.1364	.8740	.1713
2.00	1.2772	.9432	.1005	.9045	.1346
2.20	1.4677	.9604	.0729	.9283	.1047
2.40	1.6612	.9728	.0521	.9468	.0805
2.60	1.8567	.9816	.0366	.9609	.0613
2.80	2.0537	.9878	.0253	.9715	.0461
3.00	2.2518	.9920	.0172	.9795	.0343
3.20	2.4505	.9948	.0115	.9854	.0252
3.40	2.6497	.9967	.0076	.9897	.0183
3.60	2.8492	.9979	.0049	.9929	.0131
3.80	3.0489	.9987	.0031	.9951	.0093
4.00	3.2488	.9992	.0020	.9967	.0065
4.20	3.4487	.9995	.0012	.9978	.0045
4.40	3.6486	.9997	.0007	.9985	.0031
4.60	3.8486	.9998	.0004	.9990	.0021
4.80	4.0486	.9999	.0003	.9994	.0014
5.00	4.2487	1.0000	.0001	.9996	.0009
5.20	4.4487	1.0000	.0001	.9997	.0006
5.40	4.6488	1.0000	.0000	.9998	.0004
5.60	4.8488	1.0000	.0000	.9999	.0002
5.80	5.0488	1.0000	.0000	.9999	.0002
6.00	5.2489	1.0000	.0000	1.0000	.0001
6.20	5.4489	1.0000	.0000	1.0000	.0001
6.40	5.6490	1.0000	.0000	1.0000	.0000
6.60	5.8490	1.0000	.0000	1.0000	.0000
6.80	6.0491	1.0000	.0000	1.0000	.0000
7.00	6.2491	1.0000	.0000	1.0000	.0000

TABLE II.- VELOCITY AND ENTHALPY FUNCTIONS, $n = 1$ TERMS

$$\left[N_{Pr} = 0.72; \; \gamma = 1.4 \right]$$

η	f_1	f_1'	f_1''	g_1	g_1'
0	0	0	0.7946	0	0.1507
.20	.0142	.1336	.5487	.0370	.2084
.40	.0505	.2222	.3437	.0798	.2125
.60	.1006	.2738	.1783	.1198	.1835
.80	.1580	.2960	.0502	.1521	.1373
1.00	.2175	.2961	-.0439	.1743	.0852
1.20	.2754	.2805	-.1080	.1863	.0350
1.40	.3291	.2546	-.1468	.1888	-.0086
1.60	.3769	.2231	-.1652	.1834	-.0434
1.80	.4182	.1896	-.1680	.1721	-.0684
2.00	.4528	.1567	-.1597	.1567	-.0843
2.20	.4810	.1262	-.1443	.1389	-.0922
2.40	.5035	.0992	-.1252	.1202	-.0935
2.60	.5210	.0762	-.1048	.1018	-.0899
2.80	.5342	.0572	-.0850	.0845	-.0830
3.00	.5441	.0421	-.0670	.0688	-.0740
3.20	.5513	.0303	-.0514	.0549	-.0640
3.40	.5564	.0213	-.0384	.0431	-.0540
3.60	.5600	.0147	-.0280	.0333	-.0445
3.80	.5624	.0100	-.0200	.0253	-.0358
4.00	.5641	.0066	-.0139	.0189	-.0283
4.20	.5651	.0043	-.0095	.0139	-.0219
4.40	.5658	.0027	-.0063	.0101	-.0166
4.60	.5663	.0017	-.0041	.0072	-.0124
4.80	.5665	.0011	-.0026	.0050	-.0091
5.00	.5667	.0006	-.0016	.0035	-.0066
5.20	.5668	.0004	-.0010	.0024	-.0046
5.40	.5669	.0002	-.0006	.0016	-.0032
5.60	.5669	.0001	-.0003	.0011	-.0022
5.80	.5669	.0001	-.0002	.0007	-.0015
6.00	.5669	.0001	-.0001	.0004	-.0010
6.20	.5669	.0000	-.0001	.0003	-.0006
6.40	.5669	.0000	.0000	.0002	-.0004
6.60	.5669	.0000	.0000	.0001	-.0003
6.80	.5669	.0000	.0000	.0001	-.0002
7.00	.5670	.0000	.0000	.0000	-.0001
7.20	.5670	.0000	.0000	.0000	-.0001
7.40	.5670	.0000	.0000	.0000	.0000
7.60	.5670	.0000	.0000	.0000	.0000
7.80	.5670	.0000	.0000	.0000	.0000
8.00	.5670	.0000	.0000	.0000	.0000

TABLE III.- VELOCITY AND ENTHALPY

FUNCTIONS, n = 2 TERMS

$$\left[N_{Pr} = 0.72; \ \gamma = 1.4 \right]$$

η	f₂	f₂'	f₂''	g₂	g₂'
0	0	0	0.418	0	-0.096
.20	.007	.064	.229	.002	.089
.40	.023	.094	.070	.027	.145
.60	.043	.095	-.050	.055	.126
.80	.060	.076	-.130	.075	.072
1.00	.072	.046	-.172	.083	.010
1.20	.078	.010	-.181	.080	-.045
1.40	.076	-.025	-.166	.066	-.085
1.60	.068	-.056	-.135	.047	-.108
1.80	.055	-.079	-.096	.024	-.114
2.00	.037	-.094	-.054	.002	-.107
2.20	.018	-.101	-.016	-.018	-.091
2.40	-.003	-.100	.016	-.035	-.070
2.60	-.022	-.095	.039	-.046	-.048
2.80	-.040	-.086	.053	-.054	-.026
3.00	-.056	-.074	.060	-.057	-.007
3.20	-.070	-.062	.061	-.057	.008
3.40	-.081	-.050	.057	-.054	.020
3.60	-.090	-.039	.051	-.049	.027
3.80	-.097	-.030	.042	-.043	.030
4.00	-.102	-.022	.035	-.037	.031
4.20	-.106	-.016	.027	-.031	.030
4.40	-.109	-.011	.021	-.025	.027
4.60	-.111	-.008	.015	-.020	.024
4.80	-.112	-.005	.011	-.016	.020
5.00	-.113	-.003	.007	-.012	.017
5.20	-.113	-.002	.005	-.009	.013
5.40	-.114	-.001	.003	-.006	.010
5.60	-.114	-.001	.002	-.005	.008
5.80	-.114	-.001	.001	-.003	.006
6.00	-.114	.000	.001	-.002	.004
6.20	-.114	.000	.001	-.002	.003
6.40	-.114	.000	.000	-.001	.002
6.60	-.114	.000	.000	-.001	.002
6.80	-.114	.000	.000	.000	.001
7.00	-.114	.000	.000	.000	.001
7.20	-.114	.000	.000	.000	.000
7.40	-.114	.000	.000	.000	.000
7.60	-.114	.000	.000	.000	.000
7.80	-.114	.000	.000	.000	.000
8.00	-.114	.000	.000	.000	.000

TABLE IV.- ENTHALPY INTEGRAL $\int_0^\eta g_n(\eta)d\eta$

$$\left[n = 0, 1, \text{ and } 2; N_{Pr} = 0.72; \gamma = 1.4\right]$$

η	$\int_0^\eta g_0 \, d\eta$	$\int_0^\eta g_1 \, d\eta$	$\int_0^\eta g_2 \, d\eta$
0	0	0	0
.2	.022	.004	.000
.4	.070	.015	.003
.6	.149	.035	.011
.8	.253	.064	.025
1.0	.380	.095	.041
1.2	.512	.132	.057
1.4	.670	.169	.071
1.6	.823	.208	.082
1.8	1.000	.244	.089
2.0	1.18	.275	.091
2.2	1.37	.304	.088
2.4	1.54	.330	.084
2.6	1.74	.352	.075
2.8	1.92	.372	.065
3.0	2.13	.387	.054
3.2	2.32	.398	.042
3.4	2.52	.408	.031
3.6	2.72	.416	.022
3.8	2.92	.422	.012
4.0	3.12	.426	.004
4.2	3.32	.429	-.002
4.4	3.52	.431	-.008
4.6	3.72	.432	-.013
4.8	3.92	.434	-.016
5.0	4.12	.435	-.019
5.2	4.32	.436	-.021
5.4	4.52	.436	-.023
5.6	4.72	.437	-.024
5.8	4.92	.437	-.024
6.0	5.12	.437	-.025
6.2	5.32	.437	-.025
6.4	5.52	.437	-.026
6.6	5.72	.437	-.026
6.8	5.92	.437	-.026
7.0	6.12	.437	-.026
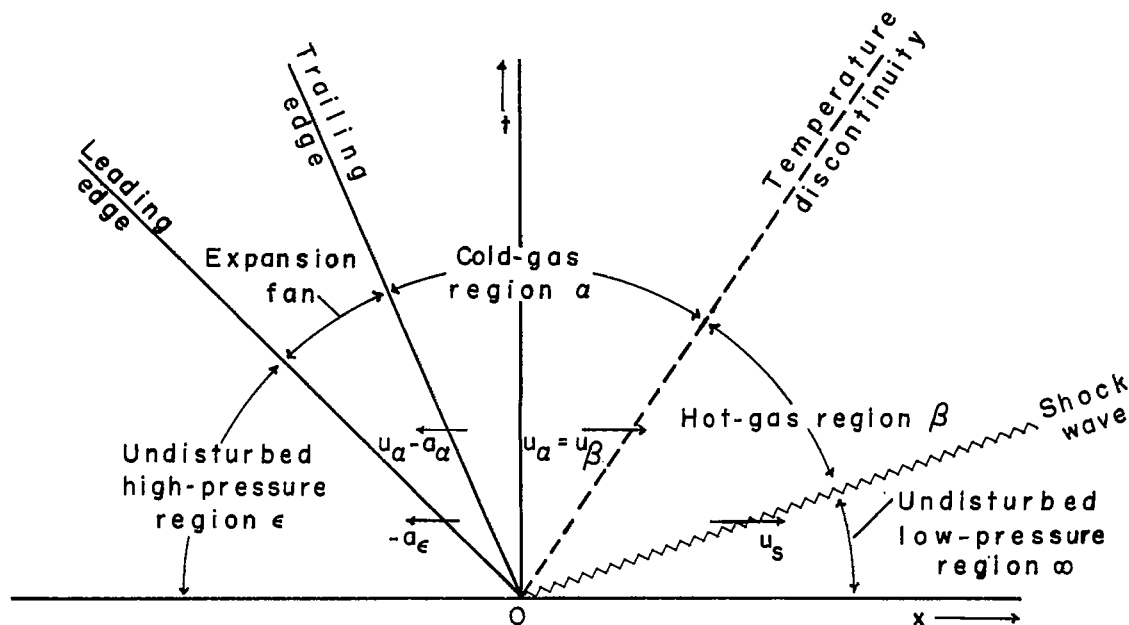
(a) Wave diagram.
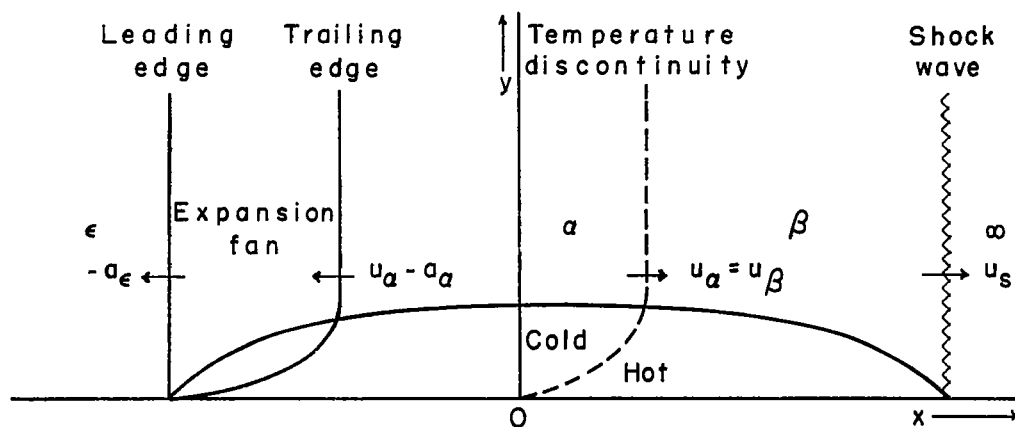
(b) Boundary layer at time t.

Figure 1.- Shock-tube wave diagram and boundary layer for expansion fan
of moderate strength.
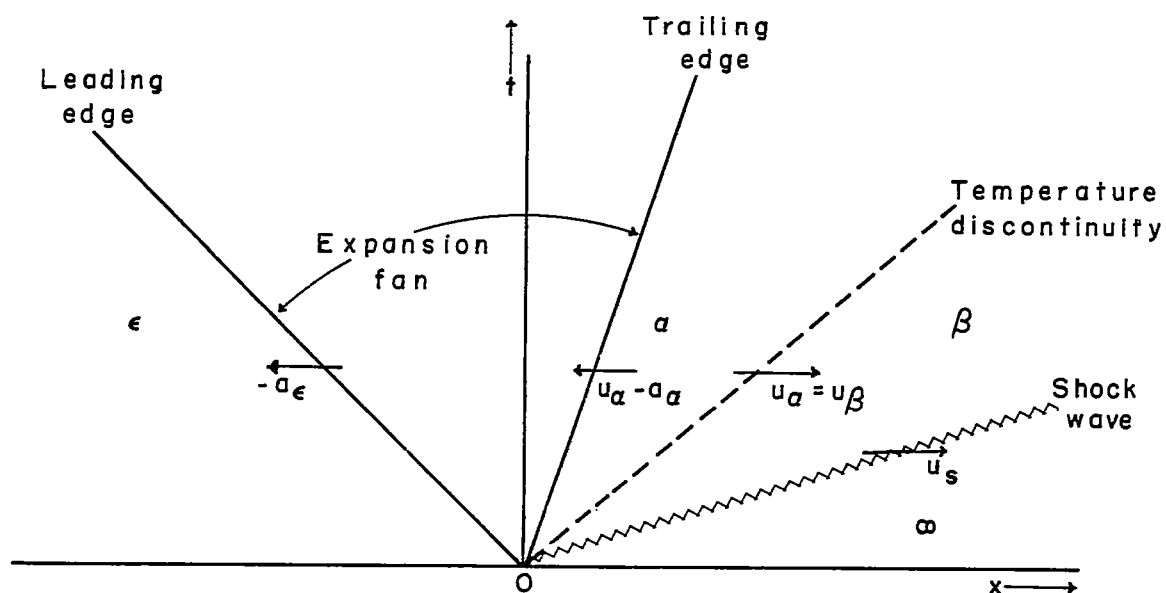
(a) Wave diagram.
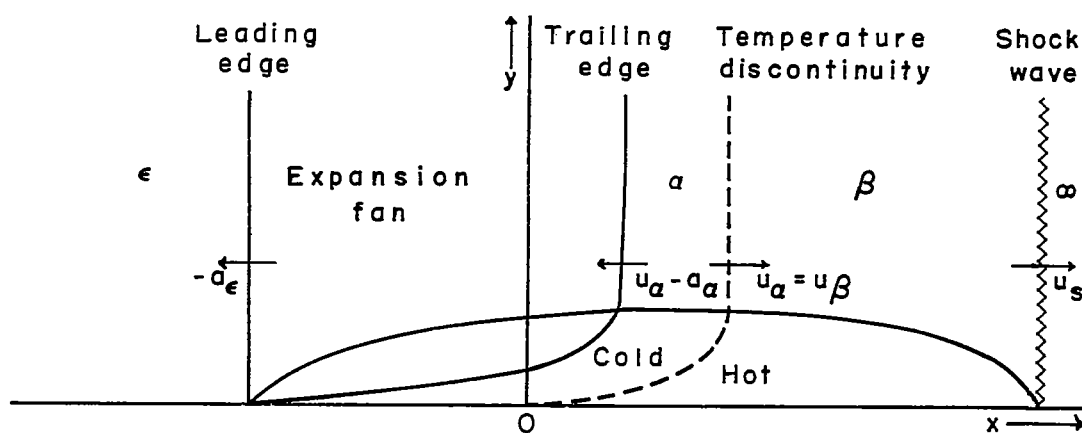
(b) Boundary layer at time t.

Figure 2.- Shock-tube wave diagram and boundary layer for strong expansion fan.
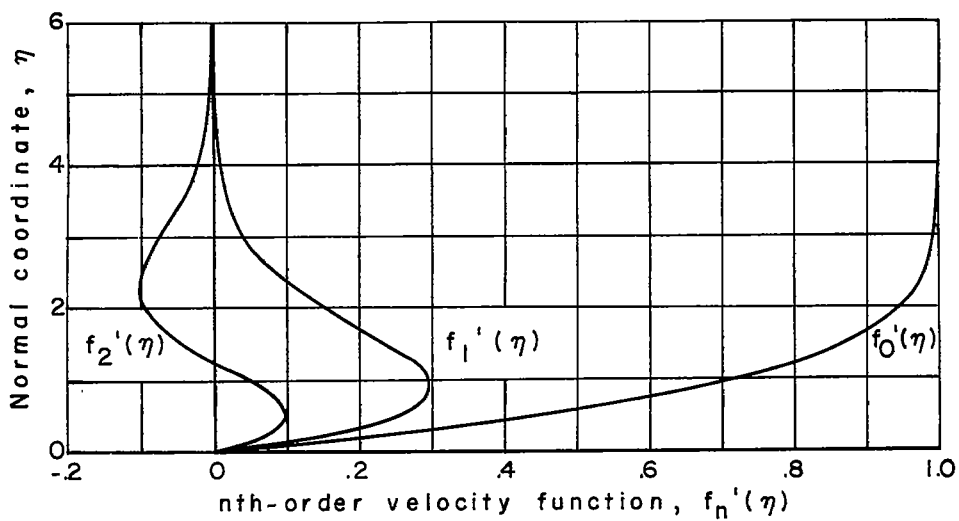
(a) Velocity functions.
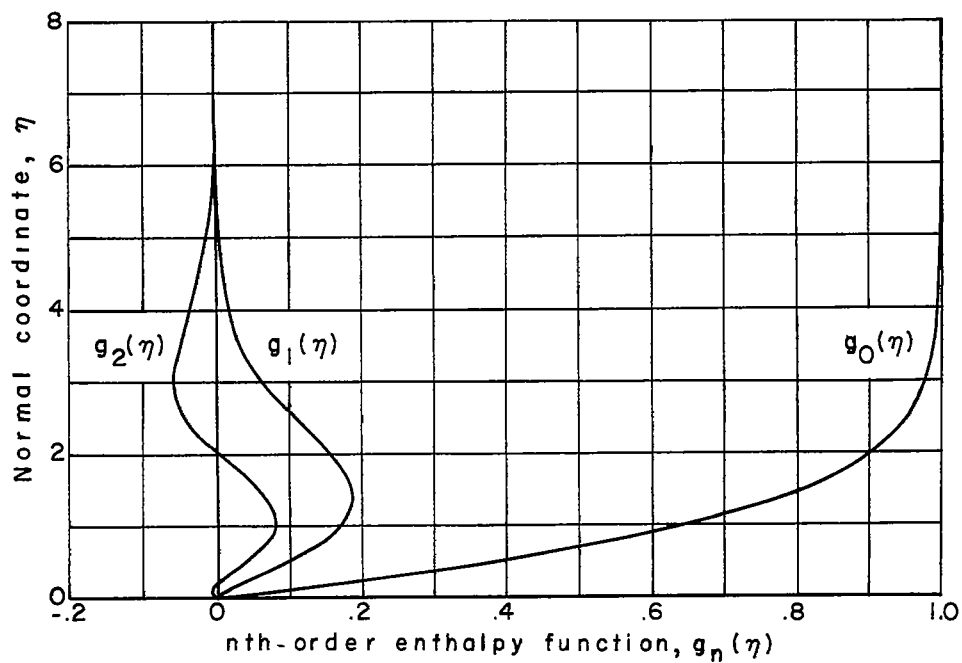
(b) Enthalpy functions.

Figure 3.- Velocity and enthalpy function profiles of the nth order. n = 0,
1, and 2.
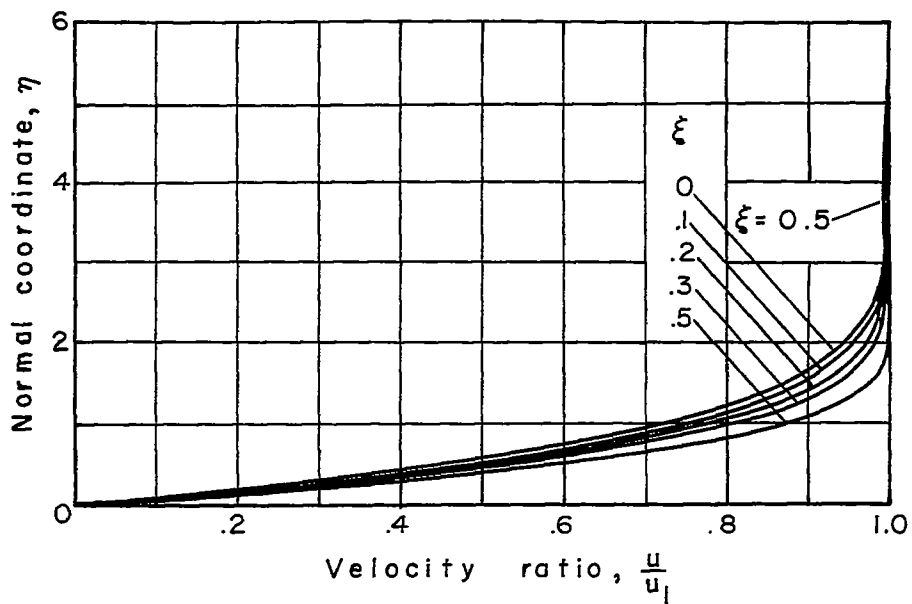
(a) Velocity profiles.
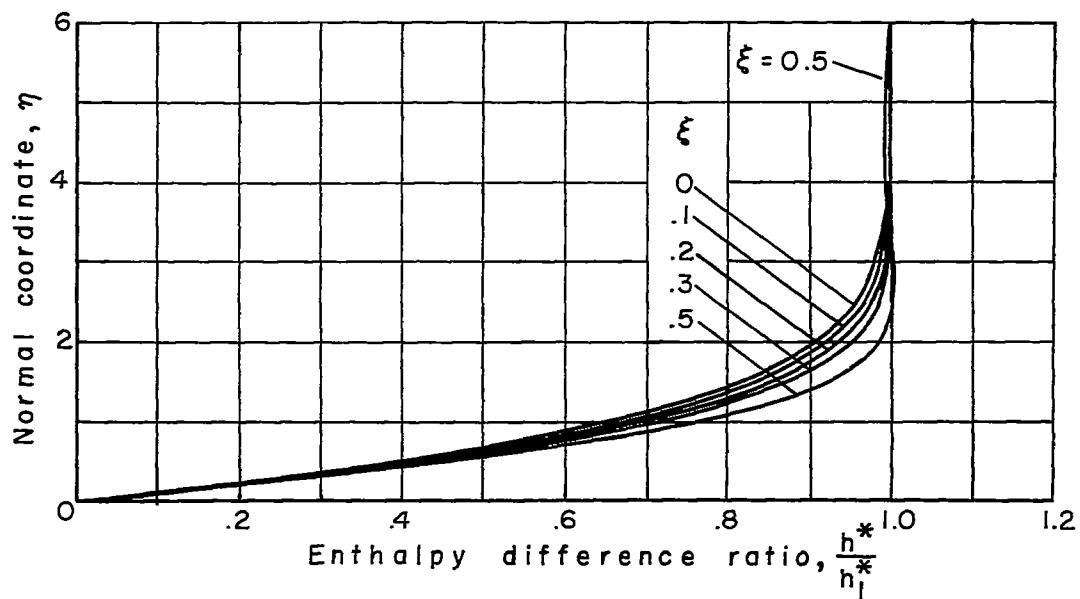
(b) Enthalpy difference profiles.

Figure 4.- Velocity and enthalpy difference profiles for various values of the conical parameter ξ.
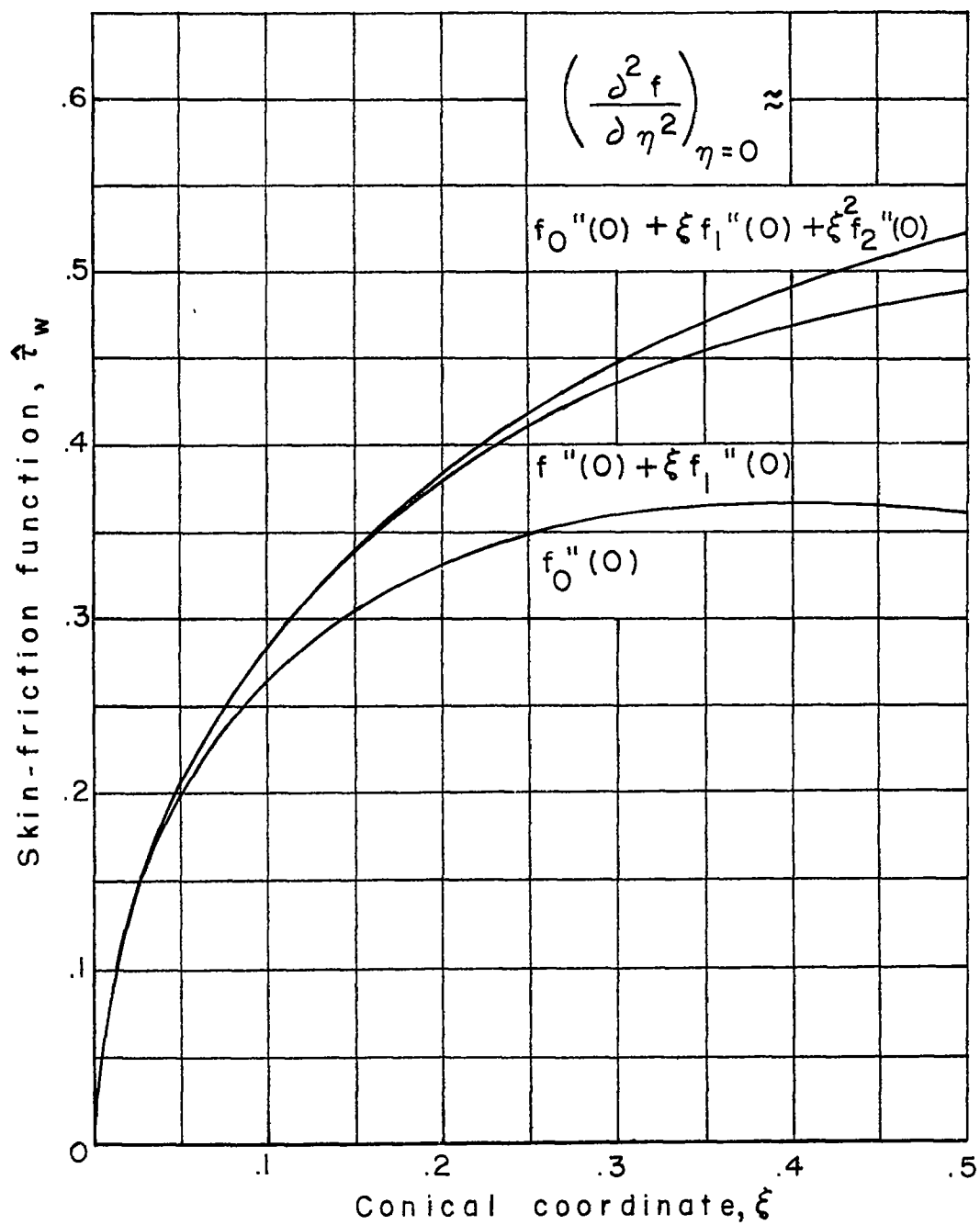
(a) Skin friction.

Figure 5.- Skin-friction and heat-transfer functions near the leading edge of the expansion fan.
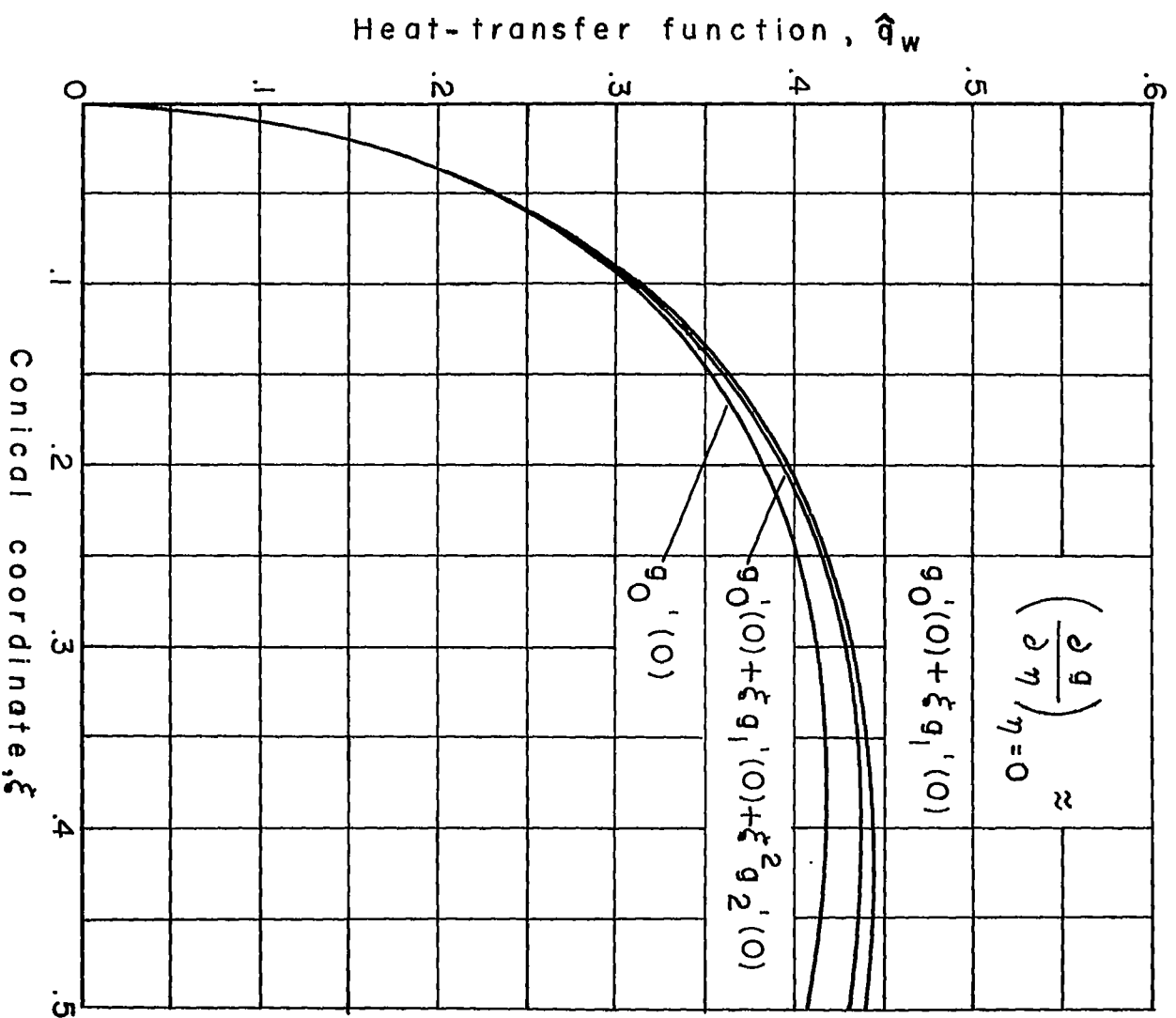
(b) Heat transfer.

Figure 5.- Concluded.
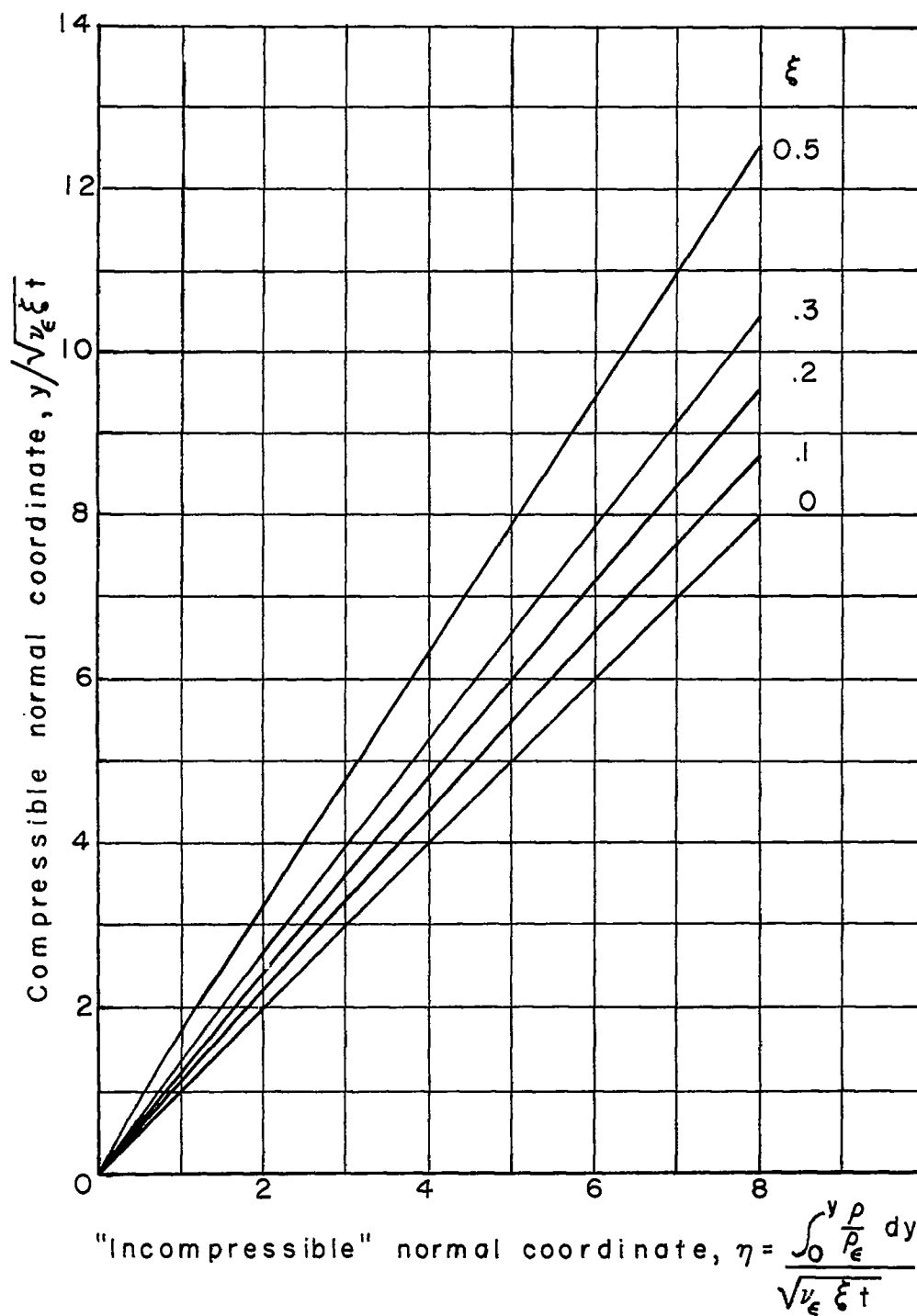
Figure 6.- Variation of compressible similarity parameter with incompressible parameter.
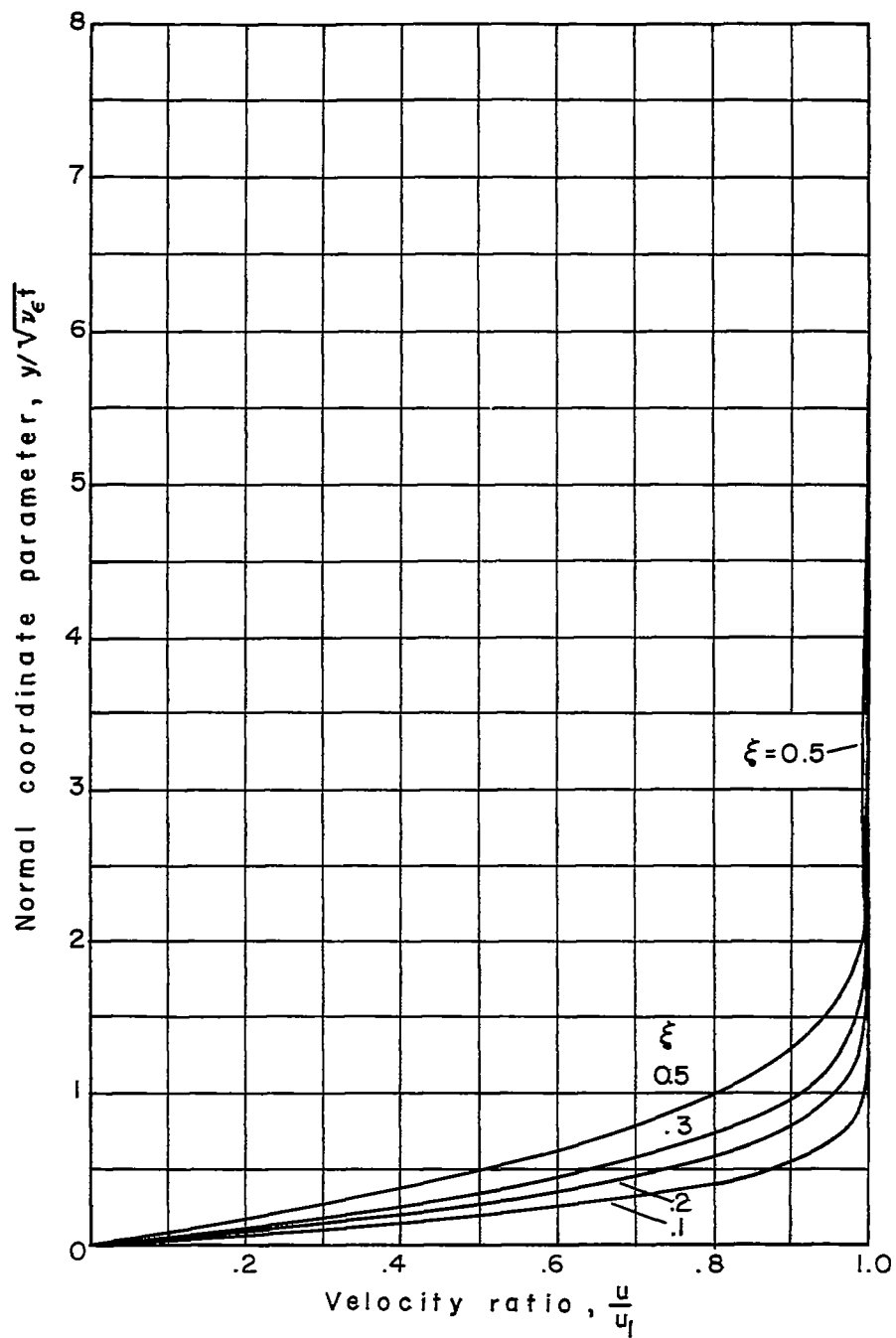
(a) Velocity profiles.

Figure 7.- Velocity and enthalpy difference boundary-layer profiles in
the physical coordinate system.
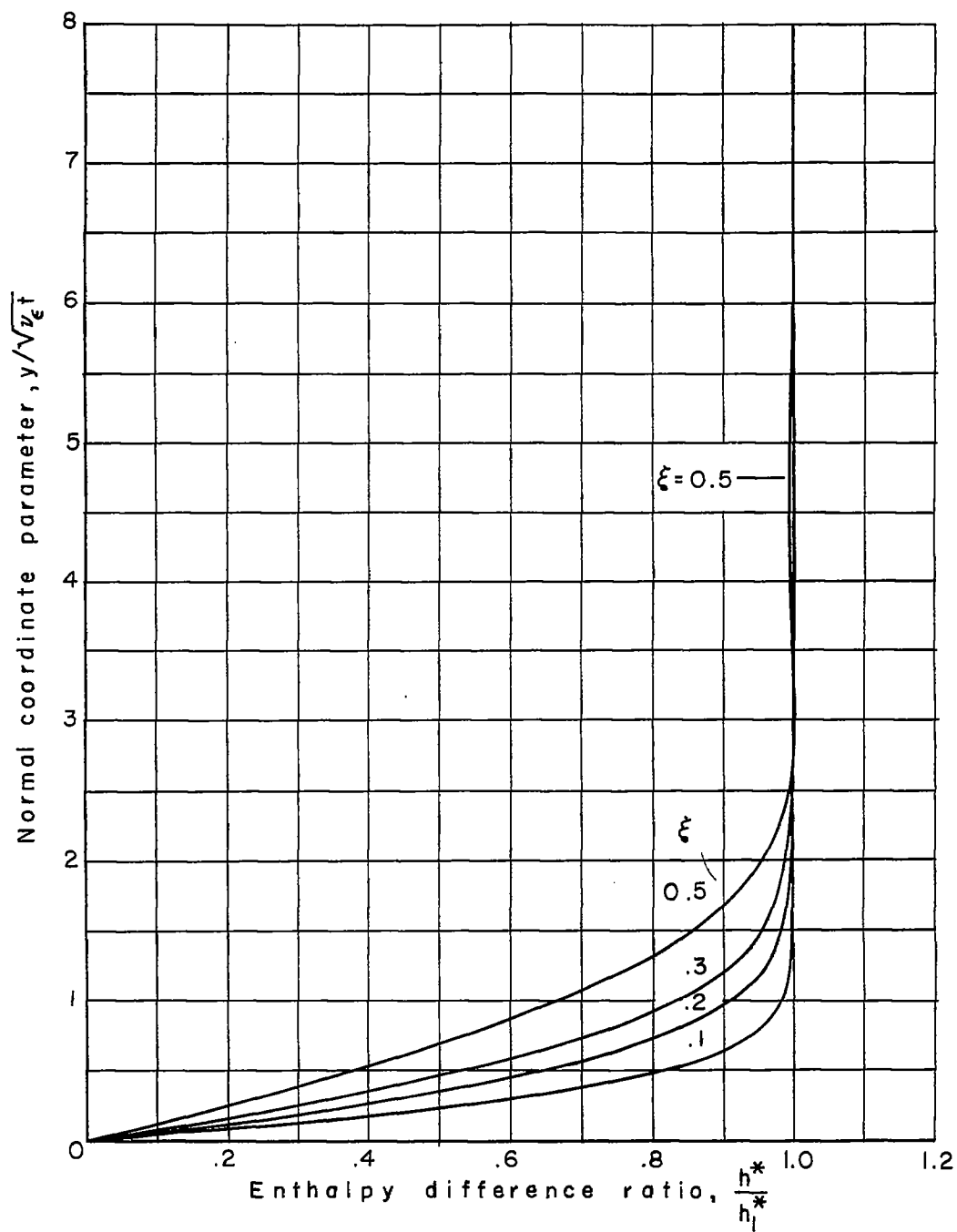
(b) Enthalpy difference profiles.

Figure 7.- Concluded.
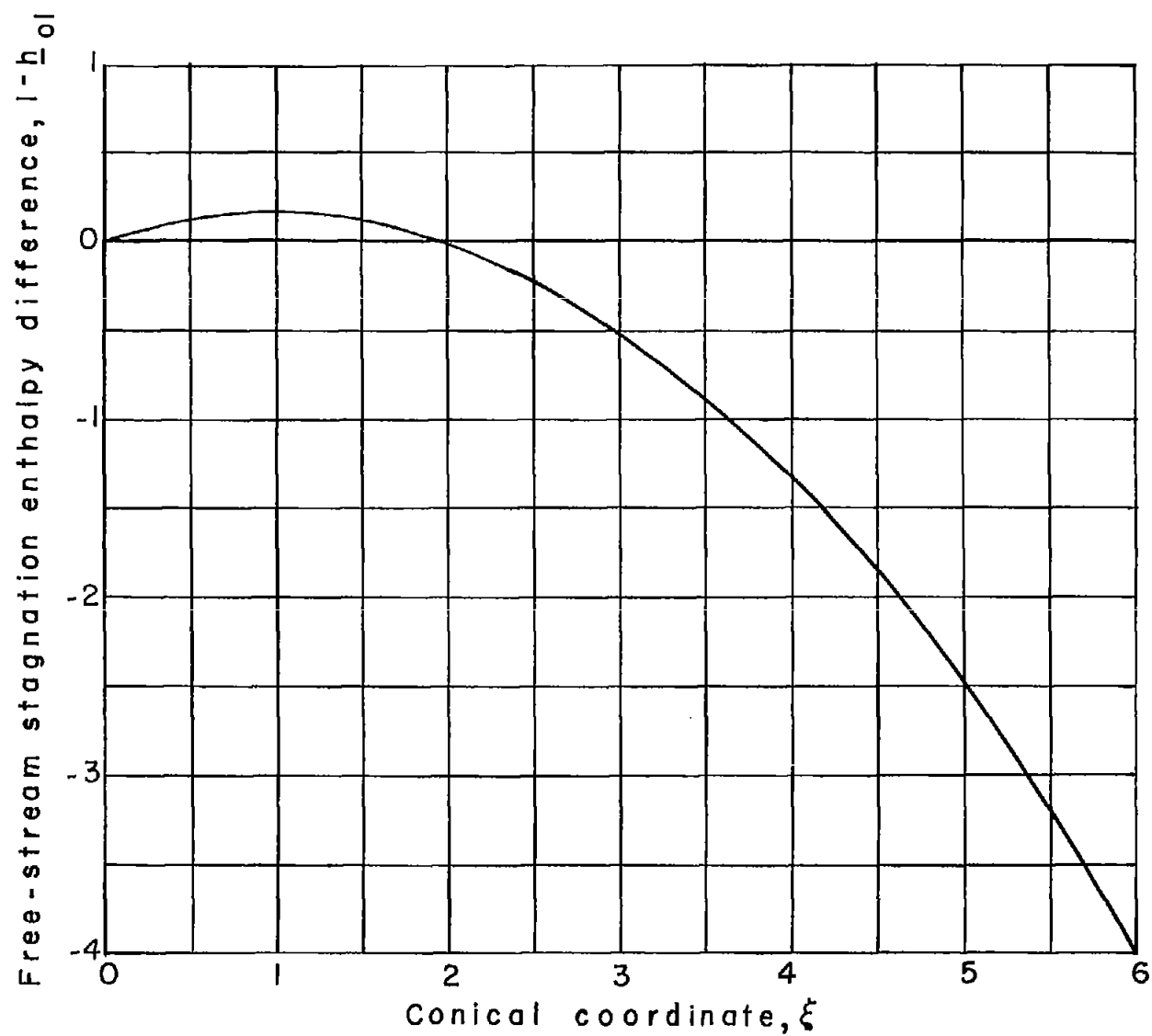
Figure 8.- Free-stream stagnation enthalpy difference in expansion fan.
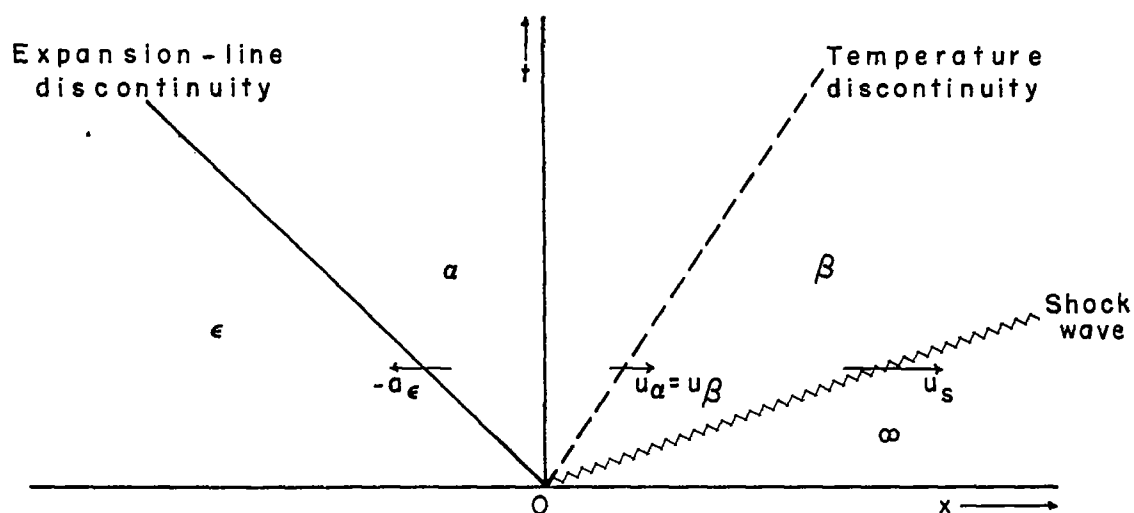
(a) Zero-thickness expansion wave.
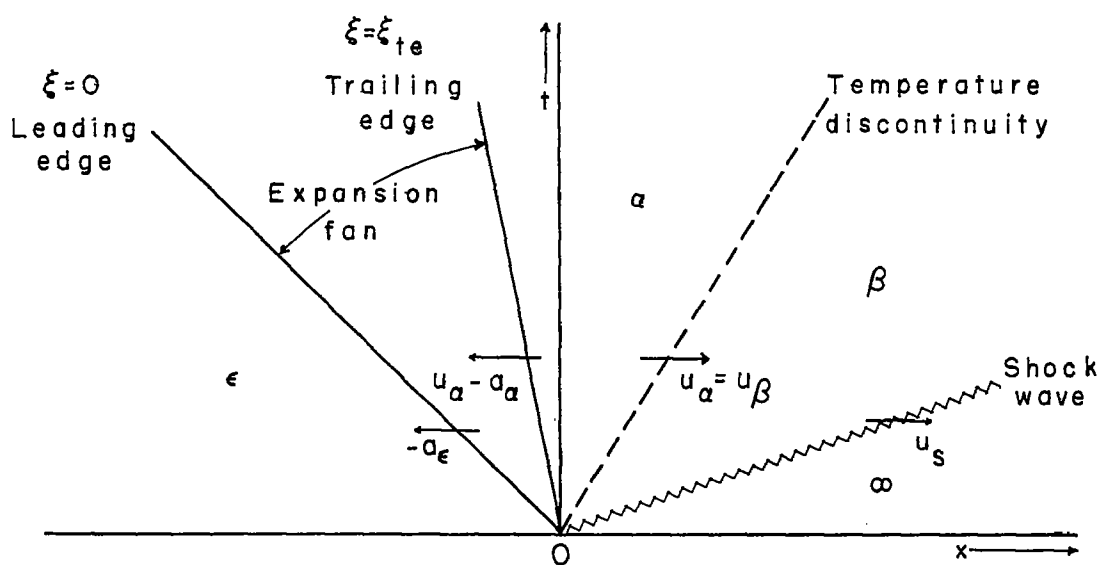
(b) True expansion fan.

Figure 9.- Typical shock-tube wave diagram for zero-thickness expansion wave and for true expansion fan.
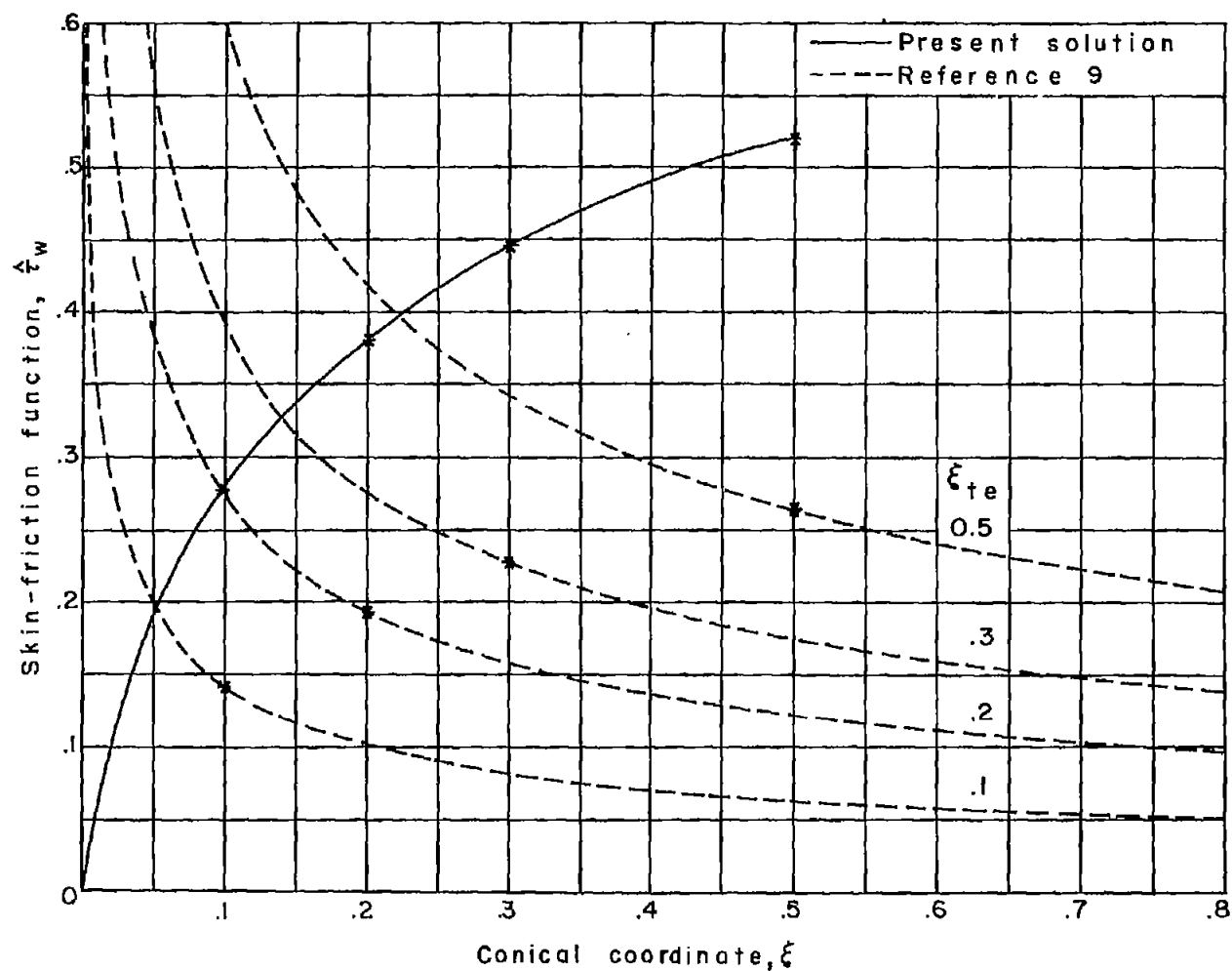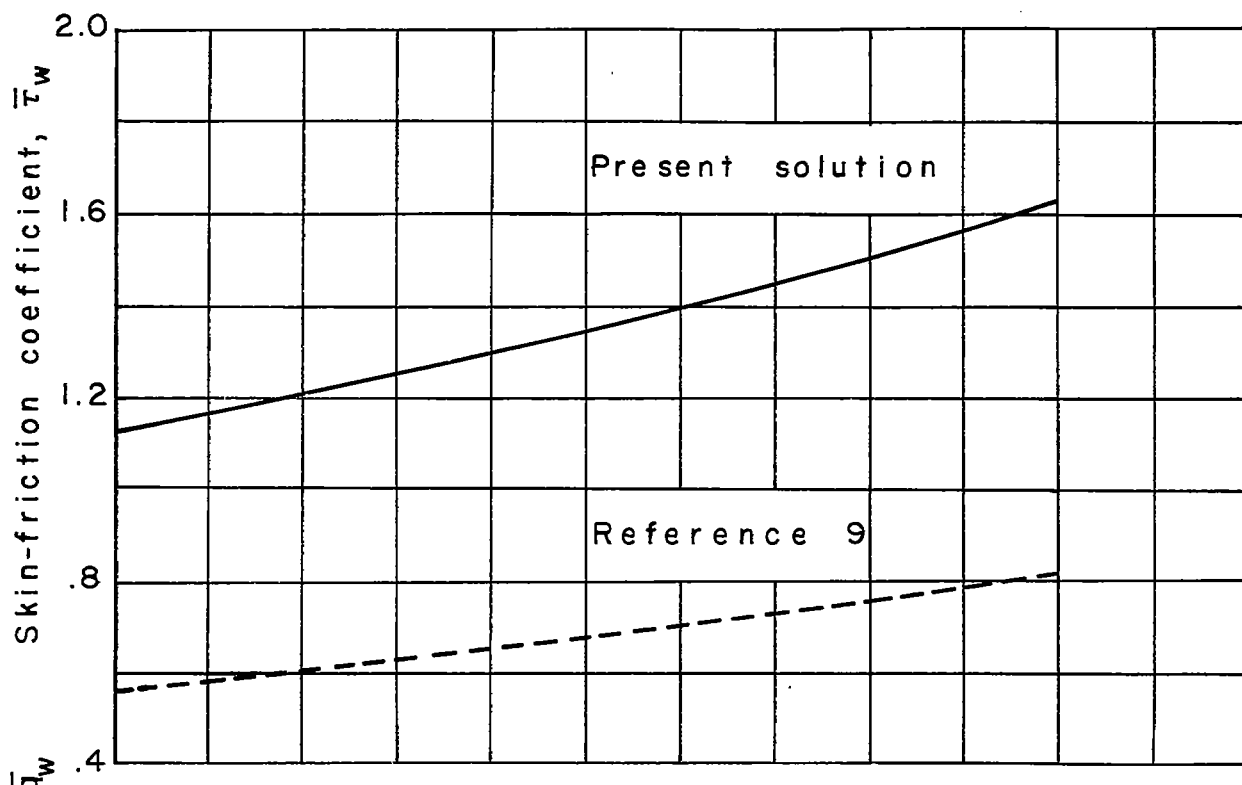
(a) Skin friction.

Figure 10.- Skin-friction and heat-transfer functions in the expansion fan compared with those for a zero-thickness expansion wave. The asterisks represent the appropriate positions of ξ_{te}.
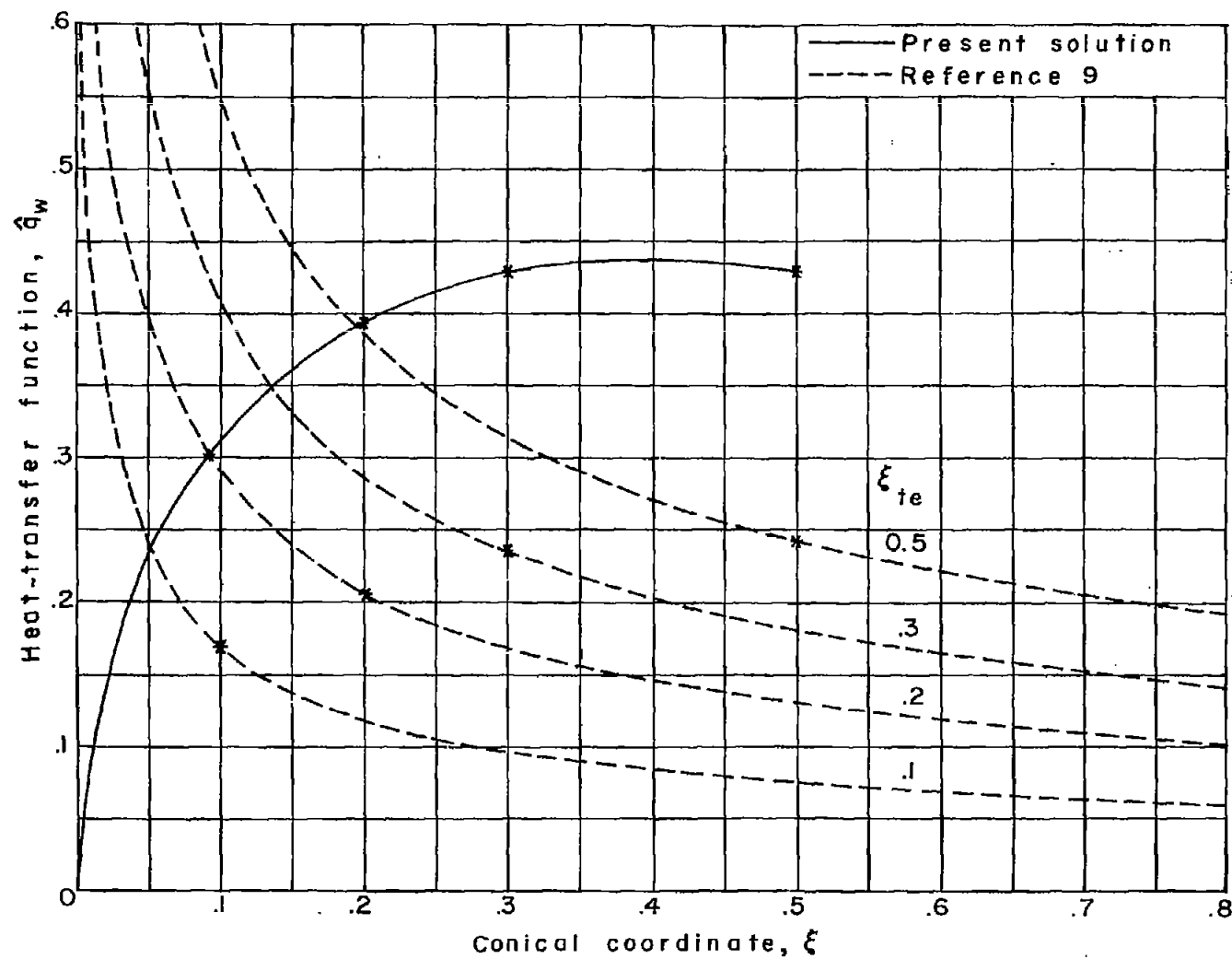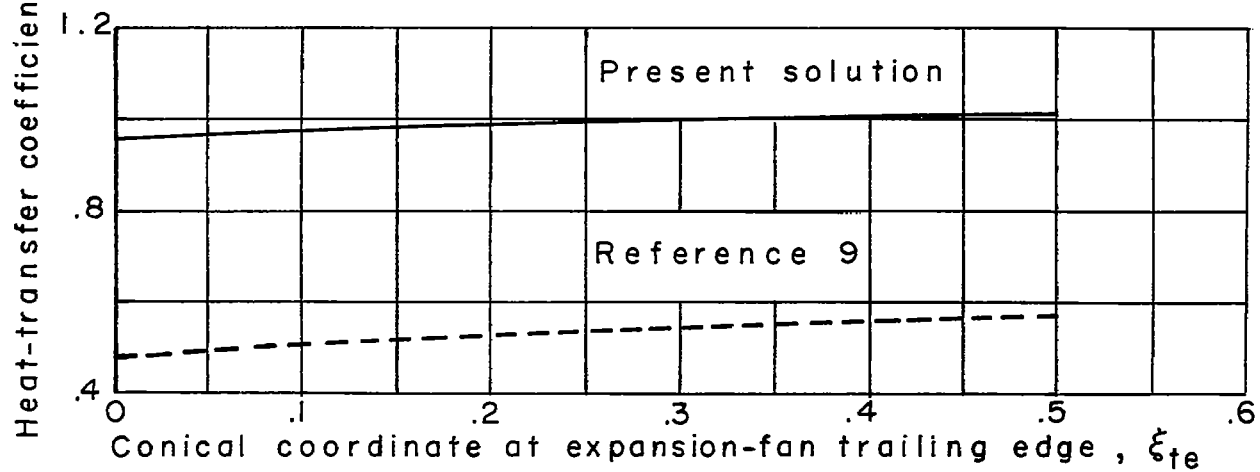
(b) Heat transfer.

Figure 10.- Concluded.

(a) Skin friction.

(b) Heat transfer.

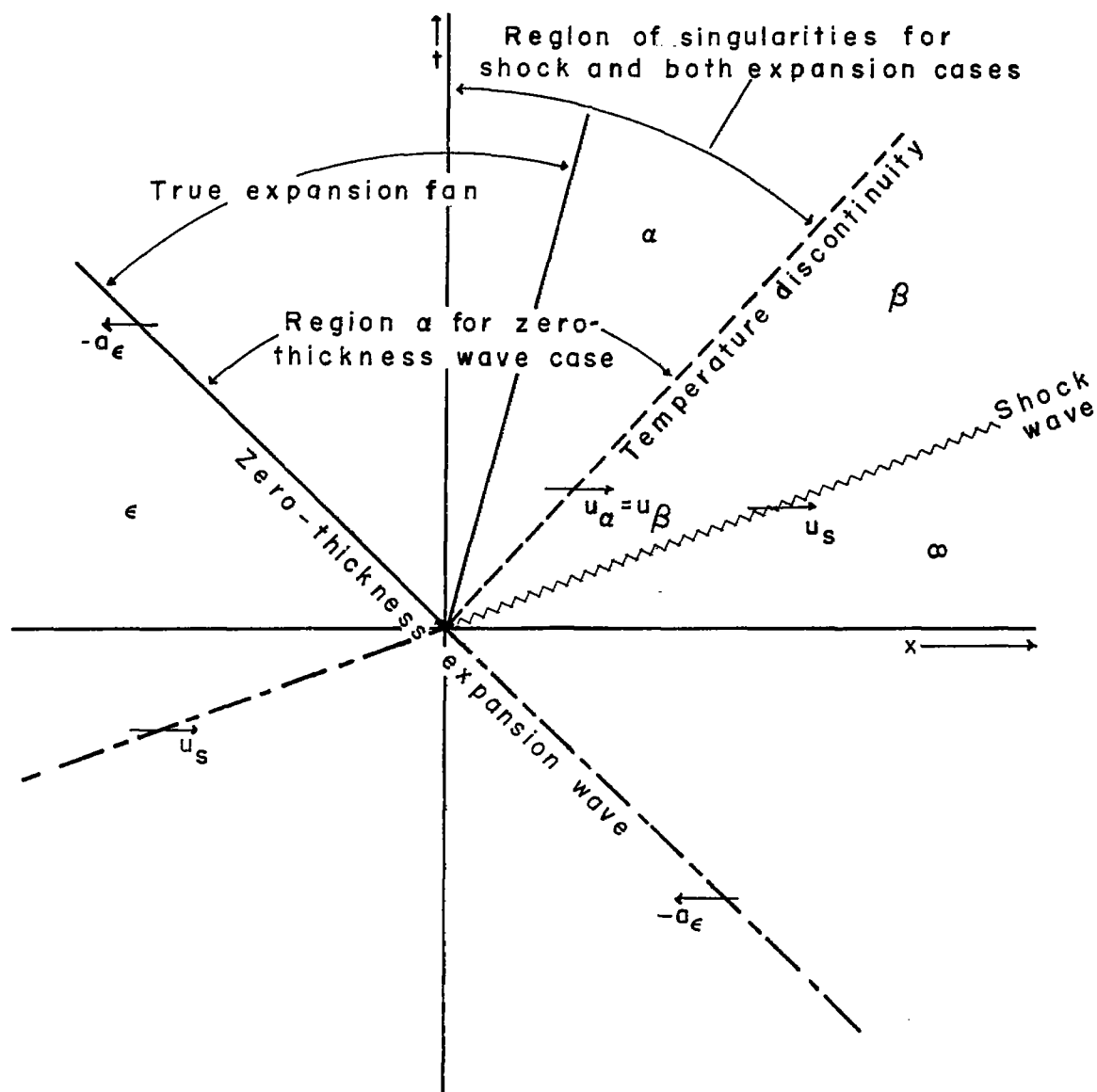Figure 11.- Skin-friction and heat-transfer coefficients for expansion
fan and for zero-thickness expansion wave.

Figure 12.- Shock-tube wave diagram.